Universiteit Leiden

Master Computer Science

Modeling the effects of matrix metalloproteinase on stressed extracellular matrix and its dysregulation in psoriasis patients

Name:	Daan Vijfvinkel
Student ID:	s2207141
Date:	July 17, 2024
Specialisation:	Bioinformatics
1st supervisor:	Prof. Dr. R.M.H. Merks
2nd supervisor:	Dr. K.J. Wolstencroft
Daily supervisor:	K.A.E. Keijzer MSc

Master's Thesis in Computer Science

Leiden Institute of Advanced Computer Science (LIACS)
Leiden University
Einsteinweg 55 2333 CA Leiden
The Netherlands

Abstract

Psoriasis is a chronic inflammatory skin disease. In the dermis of psoriasis patients a change in the fibrous extracellular matrix (ECM) structure has been noticed. Cells partake in active remodeling of their resident ECM by production of collagen and production of matrix metalloproteinases (MMPs) which digest collagen. In this thesis computational modeling is used to gain insights on the process of collagen digestion by these MMPs. An existing computational model of collagen networks and compound dynamics is extended to include experimental data about collagen degradation and the factors which influence this process. The model is tested for functionality, then is used to see how MMPs change the topology and properties of the collagen network, is perturbed to investigate how certain parameters influence the model behaviour and finally is applied to a situation mimicking the effects of a cell exerting force while simultaneously secreting MMPs. The model serves as a basis for further research on the subject of cell mediated ECM restructuring.

Acknowledgments

Thanks go out to my daily supervisor Koen, with whom I shared this journey through all its ups and downs.
Thanks go out to Roeland, whose ideas lead me to this thesis subject and an adventurous last study year.
Thanks go out to Jacky and Jake, whose fluffy companionship helped tremendously.
This work was performed using the compute resources from the Academic Leiden Interdisciplinary Cluster Environment (ALICE) provided by Leiden University.

Abbreviations and terms

CPM, Cellular Potts Model
ECM, Extracellular Matrix
MD, Molecular Dynamics
MMP, Matrix Metalloproteinase
PDE, Partial Differential Equation
TIMP, Tissue Inhibitor of Metalloproteinase
TST, Tissue Simulation Toolkit

Supplements

This thesis was submitted along with a code repository and a folder containing all relevant experiment data and code for creation of the figures in the thesis.

Contents

1 Introduction **1**
- 1.1 Psoriasis . . . 1
- 1.2 The Extracellular Matrix . . . 2
  - 1.2.1 Collagen . . . 2
  - 1.2.2 Collagen remodeling . . . 3
- 1.3 Collagen degradation rate . . . 4
- 1.4 Related work . . . 5
  - 1.4.1 Related computational models . . . 6
  - 1.4.2 Strain-degradation model generalization . . . 6
- 1.5 Research goal . . . 7

2 Methods **7**
- 2.1 Conceptual model . . . 8
  - 2.1.1 Fibrillar network . . . 8
  - 2.1.2 Collagen digestion by MMPs . . . 9
  - 2.1.3 MMP concentration dynamics . . . 9
- 2.2 Mathematical model . . . 10
  - 2.2.1 Fibrillar network . . . 10
  - 2.2.2 Collagen digestion by MMPs . . . 11
  - 2.2.3 MMP concentration dynamics . . . 12
- 2.3 Computational model . . . 12
  - 2.3.1 Fibrillar network . . . 13
  - 2.3.2 MMP concentration dynamics . . . 14
  - 2.3.3 Collagen digestion by MMPs . . . 14
  - 2.3.4 Parameter scaling . . . 17
  - 2.3.5 Simulation . . . 18
  - 2.3.6 Analysis . . . 18

3 Results **22**
- 3.1 MMPs digest the matrix locally . . . 22
- 3.2 Collagen digestion by MMP changes network topology under stress . . . 23
- 3.3 Crosslinker digestion by MMP changes network topology under stress . . . 25
- 3.4 Local MMP digestion impact depends on collagen density . . . 27
- 3.5 Strained bonds survive longer while subject to collagenase . . . 29
- 3.6 The choice of degradation law has minimal effect . . . 31
- 3.7 The value of Ξ_{min} influences digestion rates . . . 33
- 3.8 The concentration of MMP affects degradation rate . . . 35
- 3.9 Cellular contractile forces locally protect collagen against MMP digestion . . . 37
- 3.10 The amount of contractile force affects local collagen protection . . . 39

4 Discussion **40**
- 4.1 Results . . . 40

4.2 Limitations 41
4.3 Future work 43

5 Conclusion **44**

References **45**

A Effect of diffusion distance on network **52**

B Contractile force secretion radius **53**

1 Introduction

In this thesis, the goal is to gain insights in the process of collagen degradation. The motive for this is a set of observations about deviating collagen structures in the extracellular matrix of the skin for psoriasis patients. Collagen structures are changed by cells using collagen production and degradation processes. The process of collagen degradation is investigated through the use of computational modeling.
For computational modeling it is important to take into account both experimental data to base the model on, as well as the context in which the model functions: First a brief introduction is given on the psoriasis context, after which the relevant parts of extracellular matrix are explained. Finally, various aspects of collagen degradation rate and the biological models explaining conflicting experimental data are discussed.

1.1 Psoriasis

Psoriasis is a chronic inflammatory skin disease which is relatively common in the western population [1–3]. While there are various forms and variations of symptoms, such as pustular or erythematous psoriasis, the most common (about 90%) is plaque forming psoriasis (psoriasis vulgaris) [4]. Psoriasis vulgaris presents as clearly distinguishable red, rounded plaques covered with white dense skin usually described as "scales" (See Figure 1).

Figure 1: Example of scales on the hand of a psoriasis patient.
Sourced from `www.psoriasis.org/plaque`.

The disease is both associated with genetic predisposition as well as the immune system. While the debate is not fully settled, the consensus seems to be that psoriasis is an autoimmune disorder, in which the immune system overreacts to some part of the body which is falsely considered to be dangerous, usually causing damage, or in the case of psoriasis, inflammation [5]. The type of inflammation is very recognizable for psoriasis vulgaris, but no distinct immunogen has been identified which could be the target of the reaction [1, 4]. The plaques tend to form at particular places on the body which are subject to repetitive stresses such as elbows, knees or the scalp [6]. Furthermore, individuals with psoriasis

vulgaris are likely to experience non-dermatologic issues such as nail psoriasis, which expresses itself with abnormal nail growths and brittle nails, or psoriatic arthritis, in which psoriasis patients get inflammated joints, usually in the fingers [7]. There is an extensive research history and active current field on the topic of psoriasis, since it is so common and because it shows comorbidity with a few other common inflammatory and autoimmune diseases. As a result, we have discovered that the mechanics behind psoriasis are very complex. In this thesis, the focus will be on one specific aspect of these mechanics. There have been observations that the collagen structure in the extracellular matrix (ECM) of the basal membrane between the epidermis and the dermis at psoriasis plaque sites is strikingly different from regular collagen structure [8]. Since collagen is largely responsible for the elasticity of both skin and tendons (which are found in joints), this might be another avenue of approaching the problem that is the exact working of psoriasis. This idea that pathogenic circumstances such as inflammation are associated with changes in the ECM is the key starting point for the research described in this thesis.

1.2 The Extracellular Matrix

The extracellular matrix is a scaffolding surrounding, but not existing of, cells in the body. It is composed of many large molecules that form intricate structures and complexes with each other [9]. The matrix together with the cells residing in the matrix form tissues and organs. The composition and structure of the matrix and the cells within govern the shape and functioning of the tissue or organ [10]. The matrix is in constant flux, with continuous remodeling of the matrix in different ways and at different speeds keeping the body healthy and retaining homeostasis. Especially in the early stage of embryonic development during homeostasis and in many pathological circumstances this remodeling plays a key role.

1.2.1 Collagen

Collagen is the most abundant protein in animals and is the most prevalent component of the extracelullar matrix [11]. Collagen is a fibrous biopolymer protein, meaning that it is a polymer molecule consisting of monomeric subunits which are chained to form a size-variable protein that is synthesized by organisms [12]. Collagen is divided in several types (type I-XXVIII), with each type associated with different functions and tissues in the body [11, 13]. The vast majority of collagen in the human body is type I, but collagen is very versatile, manifesting itself in many different suprastructures and polymer subunit type compositions depending on the tissue. Collagen molecules consist of alpha chains which form a triple helix. These alpha chains consist of a repeated motif where each third amino acid must be glycine, which causes the chains to be tightly packed due to glycines small size [11, 14, 15]. The triple helix molecules can assemble into suprastructures, such as fibrils or networks [13]. In general, this thesis will focus on fibrillar collagen in the ECM of the skin. Fibrils in skin are usually heterotypic collagen assemblies, meaning that they are assemblies of different types of collagen molecules and that they often contain non-collagen proteoglycans which serve various regulatory functions [16].

After synthesis and secretion of individual collagen molecules by cells, fibrils are created spontaneously in the ECM adjacent to the cells. Generally it is accepted that it is a self-assembly process driven by entropy-reduction [17].

In a sense the fibrils are also a kind of biopolymers, as a suprastructure consisting of biopolymer collagen molecule subunits of variable size. The exact three dimensional process and the properties of the resulting fibril (length, thickness, composition) is not fully understood, as it depends on the type of tissue and experimental data differs both *in vitro* and *in vivo*. How the fibril molecules are organized laterally, for instance, has been a topic of extensive research without a definitive conclusion, with many different models having been proposed (i.e. [18–20]). Individual collagen molecules in the fibril are rigid due to the tight helix formation, but they are connected with covalent crosslinking, with gaps and overlap regions in the fibril structure leaving a margin for movement and through this elasticity.
This elastic property is influenced by the crosslinking level, as well as the angle in which the collagen molecules are twisted around each other in the fibril. This twist straightens out under stresses, similar to a spring [21]. Due to these molecular structural factors collagen fibrils behave spring-like, up to a certain level of force. This property is referred to as strain-stiffening [22, 23] The resulting elastic and tensile characteristics such as a Young's modulus and a Poisson curve [24, 25] are the main function of collagen fibrils, with the molecular and cellular scaffolding dictating tissue functionality depending on its mechanical properties [26]. Different tissues have different levels of stiffness due to collagen type, fibrillar composition/twist, fibril crosslinking and mineralization of collagen in the ECM [27].

1.2.2 Collagen remodeling

An important function of any type of ECM is facilitating cell motility [28], which is an important process for the skin tissue in both metastasis as well as acute processes like reaction to wounds [29]. Cell motility is among other factors dependent on the topology and stiffness of the ECM [30]; The total traction force generated by the cell is dependent on the stiffness [28] and haptotaxis through the ECM structure is vital to cell motility in the skin [29]. Through production of collagen and other constituents as described previously, cells actively shape the ECM they reside in.
Cells do not only shape the ECM by producing collagen, they also produce the enzymes necessary to degrade collagen. In humans, the collagenases of the matrix metalloproteinase family of proteins (MMP-1, MMP-8, MMP-13) are mostly responsible for enzymatic degradation of collagen in the ECM [31–34]. It should be noted that several MMPs are also active in degradation of different ECM molecules. MMPs are a part of a larger group of proteins called metalloproteases, characterized by their catalytic site containing some kind of metal, with the active site in MMPs containing zinc [34]. MMPs are secreted into the ECM by cells in a dormant inactive state. In the molecule a "cysteine-switch" mechanism is present, which is a complex between a cysteine residue in the propeptide domain of the molecule and the catalytic domain zinc atom that blocks all activity. Removal of the propeptide domain and thus removal of the cysteine from the zinc activates the MMP molecule [35]. Tissue inhibitors of metalloproteinases (TIMPs) inhibit the functioning of MMPs by inhibiting the removal of the cysteine. A complex interaction dynamic between MMPs and TIMPs drive processes in physiology, morphogenesis and wound healing; Dysregulation of the dynamic has been linked to many types of diseases which involve connective tissue [32–34, 36] and has been deemed an important factor in early tumor formation and migration [37, 38]. Through production and degradation of collagen, cells can effectively reshape the ECM. This is a process seen in morphogenesis, where rapid restructuring of the ECM is necessary (such as remodelling of bone [31]), but also in pathological circumstances, such as inflammation or cancer. In the context of psoriasis, we see symptoms of inflammation and a dyregulated ECM, which have

consequences for the mechanical properties of the fibrous collagen network, which alters cell motility and the tensile macroproperties of the skin. Because there is lacking experimental data, some other approach into gaining more insight in dynamics of ECM remodeling is necessary. For this, we turn to the field of mathematical and computational modeling.

1.3 Collagen degradation rate

In order to construct a model that produces qualitative results, quantitative input is necessary. The rate of collagen degradation by MMP is crucial for matrix restructuring and this rate is subject to different factors, such as MMP concentration, pH, temperature and collagen fibril strain. Since pH and temperature are more global factors which homeostasis aims to keep constant, MMP concentration and strain are the main parameters of influence that will be considered for the degradation rate. This also relates to the context that psoriasis plaques occur on skin areas which endure frequent and repetitive strain, with some kind of disorderly MMP concentrations. There have been a set of papers describing experiments attempting to find the different effects of the different collagenases on the different types of collagen.

The literature contains several examples of collagenase research which investigated the relation between the collagenase concentration and the degradation rate. The relation derived is unilaterally qualitatively a linear relation, but with different types of collagen and collagenases showing different values in this relation [39–44]. This means that we can assume that we deal with a first-order Michaelis-Menten reaction but that a specific Michaelis constant and slope can not determined. Simply put, more collagenase linearly causes more collagen to be degraded per timeframe, so we have a higher degradation rate.

The story is less simple for the effect of strain on collagenolysis; Generally it results from experimental data that collagen fibrils under strain are less susceptible to MMP cleavage. The exact mechanism behind the protection is not certain, but it has been speculated that it could be because the cleavage site could be more thermally stable due to straightening out the triple helix under strain [45]. It should be noted that this is not a straightforward consensus, since there has been both experimental data that conforms to this strain-protection model and data that refutes it. Additionally, the behaviour of single fibrils or fibres is not always the same as bulk mechanics of networks of fibrils. This is for instance because single fibrils can only be strained by so much before they simply break and because the dynamics between fibrils in a network is subject to intramolecular structure and variation in the suprastructure. To inform the model going forward, bulk behaviour under strain will not be considered in this thesis.

The idea that strain protects collagen from enzymatic degradation has been shown qualitatively multiple times, in experiments where fibrils which had been strained visibly survive for longer after addition of a collagenase solution [46–48]) (see for instance Figure 2). These qualititative results give a good idea to how the qualitative results might look like in the computational model.

Some of the earliest efforts for quantitavely recording the effect of strain on collagen degradation rates is by Huang and Yannas in 1977, who used a single collagen fibre (composed of crosslinked fibrils) and measured its stress levels to quantify the degradation rate by bacterial collagenase (Clostridium histolyticum) [40]. They determined rates for different collagenase concentrations, pH levels, temperatures, strain, denaturation by high temperature, crosslinking rate and inhibitor presence. Most results were used to corroborate earlier research or explain strange observations in that research. In contrast, the effect of strain on the degradation rate was a novel set of data. This data shows an almost parabolic shape, with a minimum degradation rate at 4% strain and rates increasing both with lower strain and

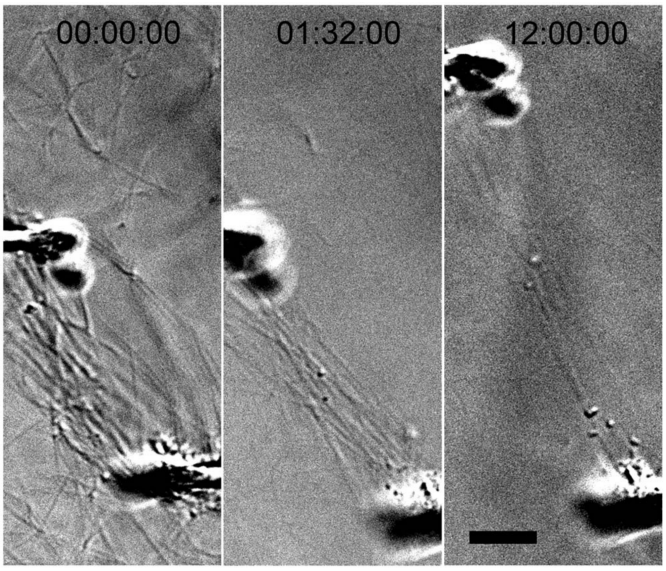

Figure 2: Snapshots of an *in vitro* experiment showing fibrils in a relaxed state, after straining with pipettes and only strained fibrils remaining after treatment with collagenase.
Sourced with permission from Flynn *et al.* [48].

higher strain. The authors speculate that higher strain levels resulting in higher degradation rates might be a result of an overstretching of the collagen triple helix opening up more sites for enzymatic attack but theorize it is probably because cleavage of one collagen molecule would result in higher stresses on neighbouring molecules causing breakage due to too high stress levels. Interestingly however, the first theory is supported in the literature, with the discovery that the collagen molecule does not fit inside the active site of MMP an "unwinding" model has been proposed [49]. This model has been experimentally supported by single trimer degradation rate research which showed that strained trimers indeed have massively higher (about 100x) degradation rates under strain [50, 51]. The unwinding model has been debated and other models have put forward [52], but this field of how the collagenase-collagen interaction works on the molecular level is considered out of scope for this thesis.
Another model, built upon experimental quantitative research that proposes there is no increase in degradation rate after increasing strain above the minimum degradation point has been introduced [53, 54]. The data that supports this model stands directly opposite to the data that there should be a rate increase at higher strains, but seems more attested by the qualitative observations. The relation gleaned from this data between strain and degradation rate seems to follow a sigmoid curve, with a certain strain point at which degradation does no longer decrease.

1.4 Related work

Now that the context of the thesis is laid out, some important related work will be highlighted. The research that will be presented builds upon two pieces of work, specifically by using an existing computational modeling framework and by incorporating collagen degradation laws generalized from the

in vitro research on collagenase degradation rates. First, some related computational models will be noted together with the model which will be extended. Afterwards, the generalized degradation laws will be explained.

1.4.1 Related computational models

This thesis will extend a computational model that has been around in some form since Merks *et al.* modeled angiogenesis and the effect of cell adhesion, cell shape and chemotaxis on this process in 2004 [55]. It contains a Cellular Potts model (CPM) which is a cell-based discrete model, originally developed for studying the effect of cell adhesion on cell sorting governed by minimization and random acceptance of nonminimization of a Hamiltonian energy function [56]. The model combines this with a partial differential equation (PDE) layer for modeling the secretion, diffusion and decay of chemotactic compounds [55, 57, 58]. This model was made into a framework environment for general CPM/PDE cell-based simulations a year later under the name Tissue Simulation Toolkit (TST) [59]. The TST has been released as an open source framework over several versions[1] and has been extended and reused in many ways. This includes modeling sprout forming of endothelial cells in angiogenesis [60], actin mediated cell movement [61] and granule morphology [62].
The specific extension that will be used as a base is the one presented by Tsingos *et al.*, which interfaces the TST with a molecular dynamics (MD) model for simulating the dynamics of a collagen fibril network in the ECM [63]. An explanation of how the relevant parts of the TST and the specific extension work is provided in Section 2.
Two other pieces of research are not directly related, but are similar in the sense of describing computational modeling of cell-ECM interactions which might be at play in our context of psoriasis and ECM remodeling with collagenase; In a study by Ristori *et al.*, the effect of repetitive strain reorienting stress-bearing collagen fibres has been computationally modeled [64]. This research lies thematically closely to the research in this thesis, by investigating how repetitive strain (such as at psoriasis plaque sites) influences individual collagen fibres and through this restructures the ECM. The way how cells respond to the ECM through mechanical feedback and the resulting behaviour of endothelial cells was modeled by van Oers *et al.* [65]. The concept of cells mechanically straining the ECM and this influencing the collective orientation and movement of cells is similar to how cells remodel the ECM with collagenase and this affecting cell movement, such is already known in cancer metastasis.

1.4.2 Strain-degradation model generalization

In their computational model incorporating both collagen degradation and production, Loerakker *et al.* generalized the experimental results of the relation between strain and degradation rate (see Section 1.3) into two distinct "degradation laws". These laws were used to simulate the remodeling of collagen in engineered tissues and in following research applied to study common loss of functionality issues in engineered heart valves [66, 67]. Generalization is necessary since while the effect of strain is quite consistent between experimental results, the exact values of degradation rate and the slope of the relation is highly dependent on other factors (such as collagenase concentration) which are not consistent between papers and experiments therein. Both generalized degradation rate laws are plotted in Figure 3.

[1] `https://sourceforge.net/projects/tst/`

The first law shown in Figure 3a is defined by

$$\frac{d(v_{\text{collagen}})}{dt} = \Xi_{\text{min}} + \frac{\Xi_{\text{max}} - \Xi_{\text{min}}}{1 + 10^{200(\varepsilon - 0.017)}}, \tag{1}$$

and constitutes the change of collagen volume v_{collagen} as a sigmoid shape between a parameter Ξ_{max} and Ξ_{min}[2] from strain ε at zero to strain ε at some given minimum degradation point, similarly to the monotonic results. The second law shown in Figure 3b is defined by

$$\frac{d(v_{\text{collagen}})}{dt} = \begin{cases} \Xi_{\text{min}} + \dfrac{\Xi_{\text{max}} - \Xi_{\text{min}}}{1 + 10^{200(\varepsilon - 0.017)}}, & \varepsilon \leq 0.028 \\ \Xi_{\text{min}} + \dfrac{\Xi_{\text{max}} - \Xi_{\text{min}}}{1 + 10^{200(0.039 - \varepsilon)}}, & \varepsilon > 0.028 \end{cases}, \tag{2}$$

and incorporates a double sigmoid, to mimic the shape of the Huang and Yannas type results. The first sigmoid goes from Ξ_{max} to Ξ_{min} just like the first law and the second is the inverse from Ξ_{min} back to Ξ_{max} when strain exceeds the minimum degradation point of $\varepsilon = 0.028$. The values of 0.017 and 0.028 are not backed up by any experimental evidence directly, but the range of strains the laws cover does generally line up with the strain values reported in the literature. This is probably because higher strain values simply cause a collagen fibril to fail under the induced stresses and break.
Both laws turned out to function identically in the implementation of their model, since the strain values never exceeded the point at which it would reach Ξ_{min}. This means there is no example of the second law in action in computational approaches and there is no precedent of these experimental results used in *in silico* models for collagen degradation. In this work we will still use both laws and examine if there is a difference in results.

1.5 Research goal

Given the previous introduction, we can now reformulate the goal of this thesis; In this thesis, the goal is to gain insights in the process of collagen degradation in the ECM of psoriasis patients by implementing the generalized strain-degradation models from Loerakker *et al.*'s research into an extension of a TST variant. The extended model can be set up, tweaked and perturbed in various ways to investigate how the parameters governing the model simulations influence the model behaviour. Through this process, different aspects of the process of collagen degradation can be explored and insight can be gained.

2 Methods

The process for creating a computational model goes through a cycle [68]. First an observation or set of observations are determined to investigate. From this a conceptual model is created to build the hypothesis. The conceptual model is the qualitative idea of which underlying processes and maybe some dynamics cause the observation. This means that this concerns a smaller scale than the observation on the larger scale. The qualitative conceptual model is then converted to a quantitative mathematical model. This involves choosing one of many paradigms or formalisms available and therein defining

[2]The original paper uses D_{min} and D_{max}. Ξ is chosen to distinguish from the symbol of D for the diffusion coefficient.

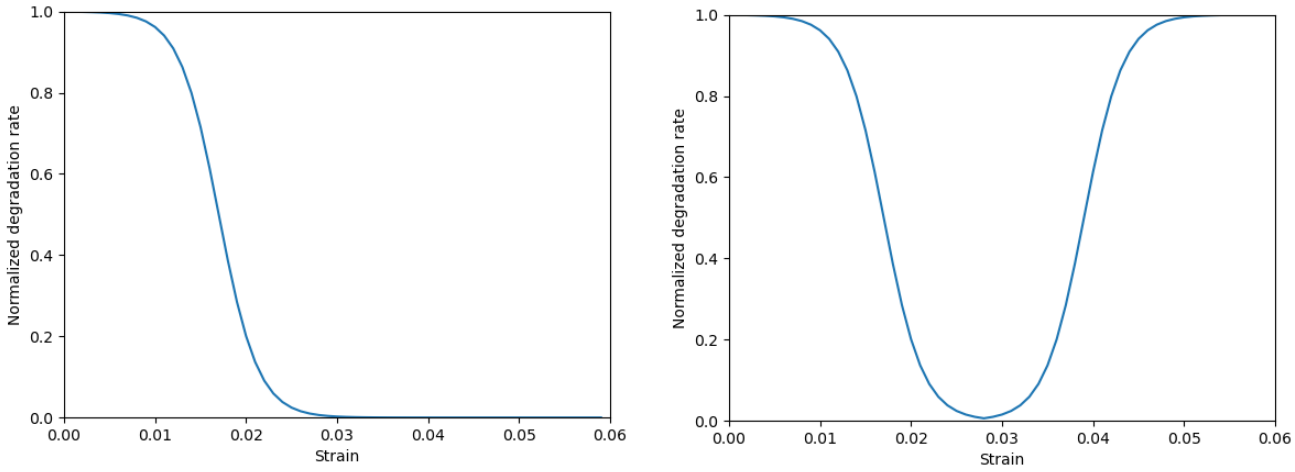

(a) **(b)**

Figure 3: Plots of the two Loerakker collagenase degradation rate laws [66]. Figure 3a shows law 1, Figure 3b shows law 2. Parameters are given in Table 1. In this figure, $\Xi_{\text{max}} = 1.0$ and $\Xi_{\text{min}} = 0.0$. The rate laws represent an abstraction from many different pieces of research providing quantitative data on the effect of strain on collagenase degradation rates (see Table 2). Since the data is not uniform, exact values can not be selected. Instead these laws act as a generalization of the relation between strain and normalized degradation rate.

mathematical rules for the processes of the conceptual model. The mathematical model is implemented computationally for experimentation. In these experiments, simulations are run to test specific aspects of the conceptual model. The results of the simulation are used to alter the conceptual model, then finetune the mathematical model, after which the model is used for new simulations in a cyclic fashion. This model cycle is an efficient way to gain insight about the functioning and behaviour of many processes and systems, both biologically and in different fields. The insight is gained through the cyclic refinement of the model, since each time the model simulations do not produce the expected results, it forces one to think about the original observations in a novel way. Note that a computational model is not infallible. A model might correctly reproduce the observation data in a way, but this does not guarantee that the underlying conceptual and mathematical model are correct as well.
In this section the models of the cycle steps are defined. The models represent the final cycle of modeling after a number of refinements throughout the research for this thesis.

2.1 Conceptual model

2.1.1 Fibrillar network

In the human skin, we observe a scaffolding of collagen fibrils forming a network that is the basis of the ECM. The network is created by the crosslinking of nearby collagen fibrils [23]. We know that collagen is largely responsible for the level rigidity and flexibility in tissues. The fibrillar collagen network in the skin lends itself to properties of flexibility and elasticity. We observe that the properties of this elasticity in regards to the stress-strain relation is similar to the way a spring behaves, with a strain-stiffening curve [21–24].
The conceptual model basis is a network of crosslinker bound collagen fibrils. These fibrils exhibit elastic

behaviour, and we want to include the strain-stiffening curve. We further ignore the other constituents of the ECM, such as proteoglycans.
We observe that for patients with psoriasis the skin forms plaques. These plaques are inflamed which leads to itchiness and irritation and importantly have less flexibility and elasticity [4]. The plaques appear more often at locations which endure frequent repetitive stresses [6]. We observe that the fibrillar network at the plaque sites has structural differences compared to regular ECM [8].
The conceptual model hypothesis contains an inkling that the changes in the fibrillar collagen network at psoriasis plaque sites are associated, either as a cause or as a result, to the pathogenic expression of psoriasis.

2.1.2 Collagen digestion by MMPs

We observe that cells have different ways to shape and reshape their resident ECM. For the focus of this thesis, collagenous fibrillar networks, this involves collagen production and collagen digestion. This thesis will focus on the digestion of collagen by cells. We observe that cells do not directly digest collagen themselves. Instead, they produce and secrete collagenase enzymes that perform this task. We observe that certain types of MMPs are mostly responsible for the degradation of collagen molecules in the ECM [31–34]. We acknowledge that MMPs and TIMPs form complex interactions of inhibition of degradation, but this thesis does not consider these dynamics. What is important however, is the observation that the degradation rate of collagen by MMPs is subject to a number of factors. The factors of interest for this thesis are MMP concentration and collagen fibril strain. We observe that there is a linear relation between collagenase concentration and the degradation rate [39–44]. We further observe that the degradation rate is strain dependent. There are two biological models to accommodate conflicting experimental results (see Section 1.4.2). The first model involves a lower strain rate for a higher strain level. The second model involves a lowering degradation rate for a higher strain level, but at a certain strain level the degradation rate rises again.
The conceptual model hypothesis involves the relations between degradation rate and both MMP concentration and collagen fibril strain levels.

2.1.3 MMP concentration dynamics

We observe that the MMP concentration and thus the degradation rate of collagen is subject to diffusion. Most compounds in the ECM undergo diffusion, where particles stochastically move from an area of higher concentration to an area of lower concentration. The highest point of concentration for MMPs are at the point of secretion, so right outside the cell membrane. The concentration at the point of secretion is determined by a secretion rate. We assume that MMP like most enzymes lose function over time. This means that the concentration is also influenced by a certain decay rate.
Diffusion can be modeled in various ways depending on the context and field of research. Which model is chosen brings with it different influencing factors on the speed of diffusion. In this thesis, only secretion rate from the cell, the characteristic diffusion coefficient and a decay rate of the MMP molecules are taken into account. The conceptual model thus involves a dynamic MMP concentration influenced by secretion rate, a diffusion coefficient and a decay rate.

2.2 Mathematical model

2.2.1 Fibrillar network

Converting the conceptual model of a network of crosslinker bound collagen fibrils with elastic behaviour leads to the modeling of collagen fibrils as a series of Hookean springs. This abstraction was made by Tsingos *et al* for the original computational model that this thesis extends [63]. Since collagen fibrils have been shown to behave spring-like in their elastic reaction to forces, Hooke's law can be applied. Since we know that collagen fibrils can also bend, the fibril is not made up of one large spring, but of a series of springs. Each of these springs has a potential energy

$$U_s = \frac{1}{2} k_s \Delta r_s^2, \tag{3}$$

where k_s is the linear spring constant and Δr_s is defined as

$$\Delta r_s = r_s - r_{s,0}, \tag{4}$$

with r_s the current length and $r_{s,0}$ the resting length of the spring. Some fibrils will be attached to other fibrils with crosslinkers. Crosslinkers are also modeled as Hookean springs as

$$U_c = \frac{1}{2} k_c \Delta r_c^2, \tag{5}$$

which is the same as fibril springs, but with its own spring constant k_c and Δr_c defined as

$$\Delta r_c = r_c - r_{c,0}, \tag{6}$$

with r_c the current length and $r_{c,0}$ the resting length of the crosslinker spring.
The way of modeling a fibril as a series of springs allows for the fibrils to bend and buckle like *in vivo*. In order to not let a fibril fold in on itself there is an angle constraint. A potential angle energy is introduced between two consecutive springs as

$$U_b = \frac{1}{2} k_b \Delta \theta^2, \tag{7}$$

where k_b is the angular spring constant and $\Delta\theta$ is

$$\Delta\theta = \theta - \theta_{b,0}, \tag{8}$$

with θ the current angle and $\theta_{b,0}$ the angular resting length.
The potential energies from the equations above result in dynamic reactions. Both stresses from fibrils attempting to achieve their resting length as well as added stresses from other sources cause movements of the fibrils. The stresses are propagated through to other fibrils through the connecting crosslinkers. The movement over time of the system is modeled using the overdamped Langevin (also known as Brownian) equation

$$\dot{X}_i = F_i + W_i, \tag{9}$$

in which W_i is a zero-mean random force.

2.2.2 Collagen digestion by MMPs

Converting the conceptual model of a collagenase degradation rate subject to MMP concentration and collagen fibril strain levels is considered while taking into account what we would want to do with the computational model experimentally. The computational model runs on discrete timesteps and thus converts a rate to a probability for each timestep. Each piece of collagen will be inspected on each timestep for inputs and receives a rate/probability to be digested. In the experiments performed, two different types of rate functions were used to gain insight on model behaviour. The first is a threshold function

$$\frac{d(v_{\text{collagen}})}{dt} = \begin{cases} 0, & c_{\text{MMP}} \leq c_{\text{th}} \\ -\infty, & c_{\text{MMP}} > c_{\text{th}} \end{cases}, \tag{10}$$

that sets the collagen degradation rate to infinity when the MMP concentration c_{MMP} exceeds the threshold concentration parameter c_{th}. In terms of probability this means the above rate equation turns into

$$P(\text{degradation}) = \begin{cases} 0, & c_{\text{MMP}} \leq c_{\text{th}} \\ 1, & c_{\text{MMP}} > c_{\text{th}} \end{cases}, \tag{11}$$

which converts the infinite degradation rate to a probability of 1.
The other type of function to be used is a strain dependent degradation function. These are Loerakker's degradation laws as defined in Equation 1 and 2. The influence of MMP concentration is interpreted by using the linear relation between concentration and degradation rate as a linear scalar c_{MMP} for the degradation rate. This works because of the foreknowledge that the MMP concentrations will be between 0 and 1 in the simulations. In terms of probability, the laws are then scaled to the length of a timestep Δt_{ex} as

$$P(\text{degradation}) = \left(\Xi_{\text{min}} + \frac{\Xi_{\text{max}} - \Xi_{\text{min}}}{1 + 10^{200(\varepsilon - 0.017)}}\right) c_{\text{MMP}} \Delta t_{\text{ex}}, \tag{12}$$

for Loerakker degradation law 1 and

$$P(\text{degradation}) = \begin{cases} \left(\Xi_{\text{min}} + \frac{\Xi_{\text{max}} - \Xi_{\text{min}}}{1 + 10^{200(\varepsilon - 0.017)}}\right) c_{\text{MMP}} \Delta t_{\text{ex}}, & \varepsilon \leq 0.028 \\ \left(\Xi_{\text{min}} + \frac{\Xi_{\text{max}} - \Xi_{\text{min}}}{1 + 10^{200(0.039 - \varepsilon)}}\right) c_{\text{MMP}} \Delta t_{\text{ex}}, & \varepsilon > 0.028 \end{cases}, \tag{13}$$

for Loerakker degradation law 2. This conversion from rate to probability is rather simple, but will later prove to be very effective for obtaining insights in model behaviour. In any future work the described rate functions could be altered or entirely exchanged for something else to investigate different types of behaviour.

In the above equations, strain (ε) is one of the variable inputs. Strain is measured differently in different fields of research (e.g. Cauchy strain in engineering) and is usually multidimensional, consisting of multiple components. For the generalized strain dependent degradation laws, Loerakker *et al.* used the linear elastic fibre strain

$$\varepsilon = 0.5((r - r_0)^2 - 1). \tag{14}$$

For simplicity, in this model only the inner part is used, so the strain on a bond is determined as

$$\varepsilon = r - r_0, \tag{15}$$

with r_0 the resting length of the spring and r the current distance between the beads. This means that the stretch to strain conversion is not exactly equal, but at the small strain levels of the models it yields the same qualitative results at slightly different values.

2.2.3 MMP concentration dynamics

Converting the conceptual model of a dynamic MMP concentration influenced by a secretion rate, a diffusion coefficient and a decay rate to a mathematical model first necessitates a way of defining where MMP is spatially located. For this a lattice space is used, with each lattice location contains a certain concentration of compound. There are three parameters necessary for the influencing factors: The secretion rate will be denoted with α, the diffusion coefficient will be denoted as D and the decay rate will be denoted as τ. The diffusion and decay dynamics are solved by a spatial partial differential equation using Euler's method

$$\frac{\partial c(x,t)}{\partial t} = D\nabla^2 c(x,t) - \tau c(x,t), \tag{16}$$

which consideres the concentration at the lattice space $c(x,t)$, the degradation of MMP with degradation rate τ and the sum of the neighbouring lattice spaces' concentration with diffusion coefficient D to determine the new concentration [55].
Some lattice spaces will be assigned as to secrete MMPs. These lattice spaces will be governed by

$$\frac{\partial c(x,t)}{\partial t} = D\nabla^2 c(x,t) - \tau c(x,t) + \alpha, \tag{17}$$

which is the previous partial differential equation with the addition of a constant secretion rate.

2.3 Computational model

The computational model implementation of the mathematical model is done by extension of an existing computational model. This model is a cell-ECM model featured in an earlier publication [63]. This model interfaces the Tissue Simulator Toolkit (TST) Cellular Potts Model (CPM) with a molecular dynamics (MD) model (see Section 1.4.1). This thesis leverages the builtin partial differential equation (PDE) layer of the TST for the MMP interaction with the collagen fibres in the MD model. Because the cell-ECM model is in continuous development by the research group this thesis was a part of, a wish for the extension implementation was that it would be largely modular. Note that the CPM part of the TST model is not used in this thesis.
This section will refer to various new parameters and parameters mentioned in Section 2.2. The parameters used in this thesis and their default values can be found in Table 1.

2.3.1 Fibrillar network

The fibrillar network as described in the mathematical model is implemented using the hoomd-blue Python package [69]. Hoomd is a high performance general purpose particle simulator, of which specifically the MD functionality is utilized. Hoomd MD supports the creation of particles with so-called "bonds" between them to exert forces. The mathematical model of considering a fibril as a series of springs is implemented as a series of "bead" particles with bonds between them that apply the potential energy as defined by Equation 3. Crosslinkers are also bonds which are created between existing fibril beads, these apply the potential energy as defined by Equation 5. Hoomd MD has an implementation of a Brownian dynamics integration method, which can be used to perform the dynamics of the network created by the bond potentials as defined by Equation 9 using a constant timestep Δt_{MD}.

Network initialization The network is always initialized the same way, similarly to the ECM model from the literature [63]; The PDE layer is initialized with size L_xxL_y. Within this same box N_{strands} coordinates are uniformly randomly chosen. For each location a random angle is chosen. At each location a bead is placed, from which $N_{\mathsf{beads}}-1$ beads are placed in the direction of the assigned random angle. The distance of the beads is defined by the fibre linear resting length $r_{s,0}$. Beads that are outside of the box can be chosen to be fixed so they will not move during the simulation by setting parameter flags. Between the placed beads, the regular fibre bonds are created. Between groups of 3 consecutive beads, angular spring potentials are added as defined by Equation 7. To form the network after generating the normal fibres, crosslinker bonds are stochastically added based on fibre density and the distance between beads compared to the crosslinker resting length $r_{c,0}$.

Linear artificial strain In most experiments some type of strain was desired to test the dynamics between strain and collagenase degradation rate. For this, the hoomd model layer was further extended to include a puller module for artificial straining. The puller receives a set of beads in the initialization phase of the model from a range from the upper PDE edge y_{pull} and stores these to pull on. Every few model timesteps as designated by a parameter the puller moves the stored beads in a given direction. Only this movement would not result in effective straining of the network however, since the pulling power of a few individual strained bonds would be dwarfed by the pulling power of the rest of the network. A feature in hoomd is taken advantage of to prevent the moved beads to be pulled back by the network while only causing negligible movement in the network itself. In hoomd, one can assign beads to be stationary and not react to any force applied. By assigning all moved beads to remain stationary after moving them, only the network will react to the stress force created by straining the bonds. In most early experiments, to prevent the network from simply moving upwards, the beads on the opposite side of the artificial strain movement were set to be stationary, effectively creating a bulk mechanics spring stretching a network consisting of many small springs. While it has been shown that bulk mechanics can reasonably be approximated by the bead-spring model in the hoomd layer [63, 70, 71], it frequently happens we do not get strain values that are all similar to the literature (between 0% and 7% strain, see the collagenase-strain experiments in Section 1.3). In most cases a majority of the fibres of interest will be within this range, so we accept the outliers.

Contractile artificial strain The puller module also supports a different type of straining. Some of the experiments will attempt to mimic the influence of a cell on the ECM by combining strain protection

and concentration scaling with a MMP gradient caused by secretion and diffusion. The simulation will not explicitly model a cell, but will model the effects a cell would have. In order to create the contractile force generated by our "cell", all beads with radius $r_{\text{min}} < r < r_{\text{max}}$ from the middle of the simulation space were selected. Between these beads and a stationary center bead a new "contractile" bond is created after the initial relaxation of the network. This is to mimic the attachment of a cell with its membrane to the ECM through a focal adhesion. The contractile bonds have a spring constant $k_{ct}$and a resting length of $r_{ct,0} = 0$, meaning that they will pull on the bead with a force until the bead is in the center of the simulation. All beads outside the PDE space are stationary and so will provide a counterforce to the contractile force. With the default value of $k_{ct} = 0.1$, the beads are pulled inwards far enough to cause straining in the network, but at some point the force of the contractile bond is equal to the force of the rest of the network pulling back, so the contractile bond will not reach it desired length of zero. Note that the puller only creates these contractile bonds once and then does not actively apply any strain to the network. The contractile bonds apply the artificial strain entirely themselves.

2.3.2 MMP concentration dynamics

The MMP concentration dynamics as described in the mathematical model is implemented using the PDE layer built into the TST program. The PDE layer contains a lattice space of size LxxLy, which is the same size as the hoomd MD layer. The TST program takes in parameters for the secretion rate (α), diffusion coefficient (D) and decay rate (τ). The user can define the secretion behaviour by selecting which lattice spaces are governed by behaviour as defined in Equation 17. The rest of the lattice spaces behave as defined by Equation 16. If desired, lattice spaces can be assigned a static value, which is used in some experiments (see Sections 3.5 to 3.8) to ensure identical and static MMP conditions in order to study certain model behaviour.

Cell secretion approximation For the experiments that mimic the effects of a cell secretion, a circle with an approximate radius of r_{max} is selected in the PDE lattice space for secretion using the midpoint circle algorithm [72]. The secretion circle radius is kept constant during the simulation. The model simulations, just like in the original paper, are considered to be a cross-section of a 3D scenario [63]. This leads to only a ring of secretion, instead of an circular area of secretion.

2.3.3 Collagen digestion by MMPs

The majority of the modular extensions created for this thesis regard the implementation of the mathematical model of collagen digestion by MMPs. The original model does not support any of this functionality, so interactions between the PDE layer and the MD layer were to be implemented as well. This "bridge" between the layers will be explained first. Afterwards the way the mathematical model was implemented will be algorithmically laid out.

Collagen mapping In hoomd, a bond is only defined by the pair of beads it exists between. It stores only the ECM bead locations and not the bond locations. Furthermore, the ECM collagen beads are stored using coordinates in a continuous real space instead of in a lattice space like the PDE layer.

This means that some method is needed to let bonds know the collagenase concentration they exist in to properly react, some way of matching spatial location in the simulation space between the two coordinate systems in the two layers.
In order to integrate collagen reactivity to MMP cleaving some solution to the difference in coordinate storage had to be found to convert coordinates from one system to the other; Either the PDE layer storing MMP concentrations had to be converted to real coordinates or the real coordinates of all fibres had to be mapped to the lattice space. The former option would lead to various considerations resulting from increasing resolution from lattice to real space, such as the question if the concentration levels would be uniform for each lattice square mapped or if some type of interpolation of concentration between two MMP squares would need to be implemented, as well as questions regarding how fine-grained the model would need to be to achieve the desired results. The latter option would reduce precision from real space to integer lattice space which needs no further considerations and turns out to be precise enough for the current model. Another big bonus is the possibility of using an existing efficient algorithm.
Every few simulation steps (with frequency set by a parameter), each bond of the MD layer is mapped to a lattice space. This means that each fibre has a position in the same system as the collagenase concentration and can react to changes in the concentration by simply inquiring the concentration at it's own lattice space mapping. This mapping is done using two different methods, depending on the type of bond that is mapped. For crosslinkers the average position of the two beads that it crosslinks is assigned as the location of the entire crosslinker. This leads to crosslinkers always covering exactly one lattice space, but since crosslinkers in the model are usually very short this is sufficient for MMP cleavage calculations. To map each bond that normal fibres consist of Bresenham's line algorithm is used [73]. Bresenham's line algorithm is a very simple iterative algorithm developed by Jack Elton Bresenham at IBM in the early days of digital computers, for use in digital plotting. The goal of the algorithm was originally to find a way to connect to points on a raster grid with only cardinal and ordinal movements, thus staying on the raster grid. Because this is such an old, simple and common algorithm, many implementations already exist. This work adapted and slightly modified a Python implementation by J.C. Craig [74]. By inserting the real coordinates of the MD layer of the two beads between a bond as inputs and correctly handling the conversion to integers we can effectively use the aliasing effect to map the bonds to the lattice space.
After the mapping is complete, each bond can be inquired about the lattice spaces it covers. This way, the program efficiently loops through each bond during the simulation process and applies digestion based on the concentration of collagenase in the covered lattice spaces. For an example of how the mapping looks, see Figure 4.

Collagen digestion Now that we have a way of linking collagen in the ECM to collagenase in the PDE layer we move to the implementation of digestion. Hoomd molecular dynamics stores different types of bonds with properties per type such as resting length and spring constant. It is also possible to "exclude" a bond from the simulation, which will remove all stresses it exerts on other bonds immediately. This function is leveraged to digest collagen in the model in a module extension which will be referred to as the excluder. Since fibrils are cleaved at once "en bloc" and the loose fibril parts then no longer can function as a stiff resistor of stresses, this instant exclusion of bonds is a reasonable approximation of the real process.

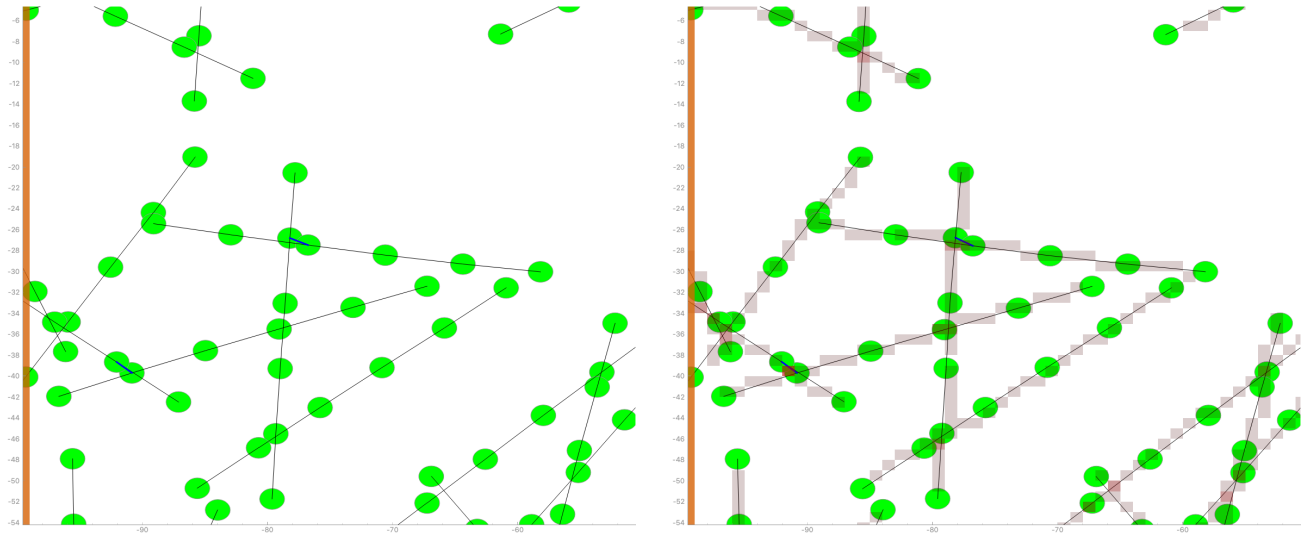

(a) **(b)**

Figure 4: An example of how the mapping of the position of bonds looks like. Figure 4a shows some bonds connected by beads. Figure 4b shows the same bonds overlaid with their lattice grid mapping. Note that lattice grid positions with more than one mapping are colored darker, such as places where there are crosslinkers.

Algorithm 1: Digestion framework algorithm

Input : all bonds

```
for bond in allbonds do
    if excludebondtype(bond) then
        strain = ||bead2 − bead1||− restlength;
        concentration = 0;
        n_lattice_spaces = 0;
        for lattice space in bond occupied lattice spaces do
            concentration = concentration + lattice_space_concentration;
            n_lattice_spaces = n_lattice_spaces + 1;
        end
        concentration = concentration / n_lattice_spaces;
        if f(concentration, strain) then                    // interchangeable function f
            exclude bond from hoomd model;
        end
    end
end
```

The digestion rate of collagen in the model is determined by the mathematical model equations. The main functionality is digestion dependent on both the concentration of collagenase and the strain on the fibrils *in vivo* and *in vitro*. The exact parameter values can be varied to tune the model, but the overall framework of how the digestion algorithm works stays the same, which can be seen in Algorithm 1.
The digestion algorithm is fully modular. The function can be called to run for a certain amount of

simulation time and can optionally digest crosslinkers, fibrils or both. When the function is called, the algorithm loops through every bond in the simulation domain which is not yet digested. Each bond knows which lattice spaces it occupies due to the mapping applied earlier, so we can inquire the occupies lattice spaces in the PDE layer about the collagenase concentrations. The average concentration of the lattice spaces is considered to be the concentration of collagenase the fibril endures. *In vivo* and *in vitro* the collagenase will at some point cleave exactly one location on the fibril, but since the model resolution does not lend itself to this, the abstraction of digestion of the bond due to the average concentration over the entire bond is made.
When both influencing variables are calculated the collagenase concentration and strain are passed to a probability function. The probability function is interchangeable depending on the type of simulation that is to be run. The function used in this thesis are defined by Equations (11) to (13). The function should return a value between 0 and 1, telling what the chance is of cleavage by digestion of the bond. A random number is rolled and when it is lower than the function value hoomd is instructed to exclude the bond from further simulations, effectively breaking the fibril. Note that in the simulation the strain can also be negative, meaning that the length of the bond is less than the resting length. There is no information anywhere in the literature about collagenase degradation rates under negative strain. Thus, in the case of a negative strain in the simulation, the breaking chance is simply assumed to be 1, so negative strain bonds are always digested immediately.
When taken over many timesteps the chance returned by the function is equal to the degradation rate. After looping through all bonds, some cleaning up is done by removing all beads which have no bonds connecting them to other beads due to digestion. Computationally, the more digestion is done, the faster the simulation runs due to hoomd no longer needing to simulate the digested bonds and beads and the digestion algorithm looping through less bonds.

2.3.4 Parameter scaling

With the mathematical model components implemented into computational model layers and functionality, the model works on its own. We do want to somehow link the behaviour of the model to actual behaviour, so units of the model need to be converted to actual measurements and units. This is done through parameter scaling. In the parameter table Table 1, the column "TST value" regards the parameter values used as input for the computer program, while the column "Default value" considers the scaled values with units. An explanation of how the parameters are scaled is in order.
In an *in vitro* experiment, the diffusion of collagenase, the stressing dynamics of collagen in the network and the cleavage of collagen fibrils by the excluder would happen simultaneously. *In silico*, each of these steps calls a different algorithm and need to be done consecutively, so some type of concession needs to be made. In the main simulation loop of the model, the algorithms in the PDE, the hoomd network and the excluder are assigned a certain time they are to simulate for and follow each other up to form one timestep. This is similar to how simulation of simultaneous processes have been modeled in CPM extensions previously [63, 65].
Space and time are the starting point for most of the conversions made. The first assumption is taken from the original model, which determines that each lattice space is 0.25x0.25 μm^2. This results in rather simple scaling for all spatial parameters. All ECM parameter scalings regarding force are directly taken from the original model and their values from the parameter table in the paper introducing the model in order to be consistent with the spatial scaling. Time scaling was chosen by setting each main

loop timestep to be 0.2 seconds long ($\Delta t_{\text{MD}} * t_{\text{MD}} + \Delta t_{\text{ex}}$). This time scaling means that each timestep is about an order of magnitude smaller than the original model and was chosen to more closely inspect the impact of the digestion of MMP and the sudden removal of stresses in the ECM.
The PDE parameters are a result of the spatial and temporal scalings. While the previous scalings separately reasonably translate to the real world, the PDE parameters do not. The scaled diffusion coefficient for example, is extremely small compared to what one would expect based on experimental values on MMP diffusion. Both the secretion rate of MMPs by cells and the decay rate of MMP have no data in the literature, so the values are inferred and can not be compared to confirm or deny if they are reasonable.

2.3.5 Simulation

Now that the model functioning is laid out, we proceed to an explanation of how simulations are run using the model program. The simulations generally follow three phases: initialization, straining and degradation. A diagram of the entire simulation can be seen in Figure 5. This setup is inspired by the *in vitro* experiments on collagen degradation rate (see Section 1.3). In those experiments, collagen networks or singular fibrils are relaxed, then artificially strained and finally subjected to collagenases. The ECM MD network functions with a step size of Δt_{MD}. In the simulation, the ECM network is generated as described in Section 2.3.1 and then given ample time (t_{MDinit} steps) to relax into a mechanical steady state. After initialization, the simulation proceeds in simulation steps. During straining, each simulation step starts by straining the network once and then letting the network relax for t_{MDstrain} steps. This happens for T_{strain} simulation steps. At the end of the straining phase, the network is once again relaxed for a longer time (t_{MDrelax} steps) to move towards mechanical equilibrium. During the last phase of degradation, MMP is added to the simulation and a timestep consists of integration of the ECM followed by a single step (t_{ex}) of excluder digestion (as described in Algorithm 1). The excluder functions with a significantly larger step size Δt_{ex} and the amount of MD integration timesteps during digestion t_{MD} is smaller than earlier in the simulation, to model the fact that molecular digestion happens on a significantly faster timescale than the mechanical larger scale movement of the ECM reaction.

2.3.6 Analysis

In the following section regarding the experiments and their results the model is both qualitatively and quantitatively analyzed.
For qualitative analysis the model exports images after each simulation timestep. The image shows the PDE layer with concentration levels of MMP in a cyan color with corresponding color intensity to the concentration and an orange outline around the PDE field. If desired, the concentration levels are shown in magenta using the CONREC level contouring algorithm by Paul Bourke [76]. Layered on top of the PDE image is a display of the ECM in the hoomd layer. Fibril bonds are drawn as black lines, crosslinker bonds are drawn as thick blue lines. In the later experiments with contractile bonds the contractile bonds are drawn as thin yellow lines.

For quantitative analysis, the model exports data about the ECM each simulation timestep regarding the positions of beads and which beads are connected by which bonds. This raw data is used for lifetime

Parameter	Default value	Description	Source	TST value
Simulation space				
Lx x Ly	50 x 50 (μm^2)	PDE layer simulation space size	base model	200 x 200
Hx x Hy	87.5 x 1000 (μm^2)	Hoomd network simulation space size	chosen	350 x 4000
ECM				
N_{strands}	2000 (-)	Number of strands initialized	base model	2000
N_{beads}	9 (-)	Number of beads per strand	[63]	9
N_c	2000 (-)	Maximum number of crosslinkers	chosen	2000
$r_{s,0}$	1.5625 (μm)	Fibre bond linear resting length	[63]	6.25
k_s	3.1 x 10^{-3} (N m^{-1})	Fibre bond linear spring constant	[63]	200
$\theta_{b,0}$	π (-)	Fibre angular resting length	[63]	π
k_b	6.1 x 10^{-18} (N m rad^{-1})	Fibre angular spring constant	[63]	200
$r_{c,0}$	0.4 (μm)	Crosslinker bond resting length	base model	1.6
k_c	3.1 x 10^{-3} (N m^{-1})	Crosslinker bond spring constant	base model	200
PDE				
D	1.5625 x 10^{-13} (μm^2 s^{-1})	Diffusion coefficient	[75]	5e-13
τ	0.002 (s^{-1})	Decay rate	base model	0.0004
α	0.18 (s^{-1})	Secretion rate	chosen	0.036
Puller				
y_{pull}	5 (μm)	Linear pull range	chosen	20
Δy	0.25 (μm)	Linear displacement applied to network	chosen	1
r_{min}	7.5 (μm)	Contractile minimum bead selection radius	chosen	30
r_{max}	12.5 (μm)	Contractile maximum bead selection radius	chosen	50
$r_{ct,0}$	0 (μm)	Contractile bond linear resting length	chosen	0
k_{ct}	1.55 x 10^{-6} (N m^{-1})	Contractile bond linear spring constant	chosen	0.1
Excluder				
Ξ_{min}	0.0 (-)	Loerakker laws minimum degradation rate	chosen	0.0
Ξ_{max}	1.0 (-)	Loerakker laws maximum degradation rate	[66]	1.0
Time				
Δt_{MD}	0.00001 (s)	Timestep for molecular dynamics integration	chosen	0.00001
t_{MDinit}	800000 (-)	MD integration steps during initialization	chosen	800000
t_{MDstrain}	100000 (-)	MD integration steps during straining	chosen	100000
t_{MDrelax}	400000 (-)	MD integration steps after straining	chosen	400000
t_{MD}	10000 (-)	MD integration steps during degradation	chosen	10000
Δt_{ex}	0.1 (s)	Timestep for excluder degradation	chosen	0.1
t_{ex}	1 (-)	Excluder steps during degradation	chosen	1
T_{strain}	80 (-)	Amount of simulation steps during straining phase	chosen	80

Table 1: Table of parameters used by the computational model. For each parameter, the default value is listed. Unless specified otherwise, this default value is used in all simulations. The second column notes the scaled paramaters with corresponding units, the last column notes the value used in the computer program that runs the computational model (TST). Note that the base model heavily relies on the model by Tsingos *et al.* [63] and the model by Merks *et al.* [55], but the specific parameter settings listed in the papers introducing the models were mostly not the same as the model used as a basis for this thesis because the model is in continuous development. A distinction is made by either referencing the paper directly or mentioning "base model" as a source.

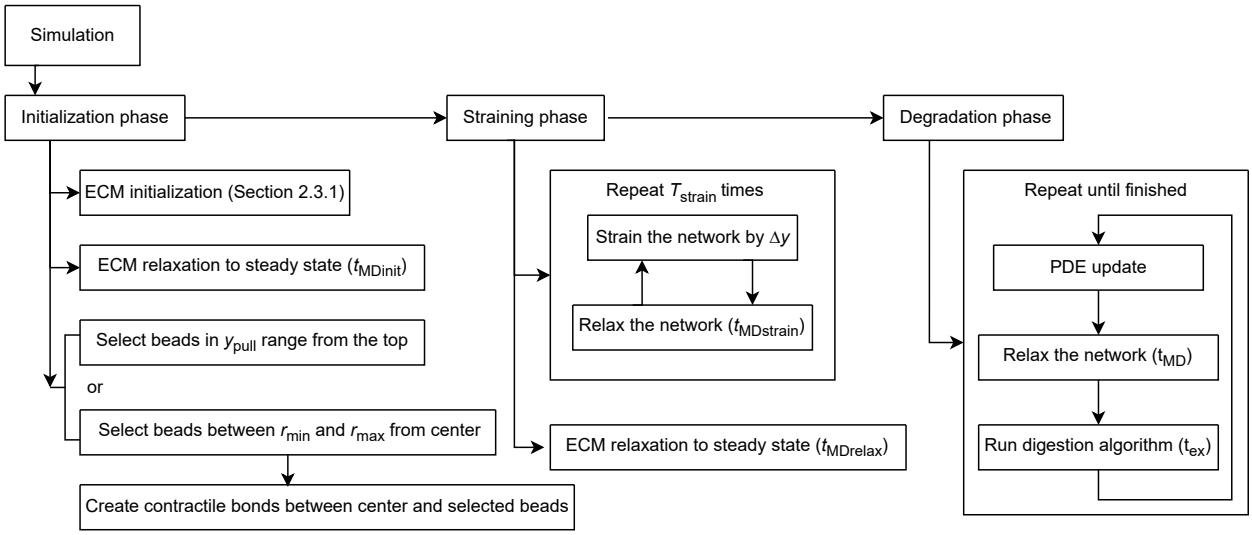

Figure 5: Flowchart diagram of the simulation process in the computational model. First the initialization phase runs with ECM initialization, ECM relaxation and bead selection for artificial strain. Then in the straining phase these selected beads are moved to create artificial strain, alternated with a relaxation of the network to let the artificial strain take effect in the network. Finally in the degradation phase MMP is added through the PDE layer. This phase loops through a PDE update, relaxation of the network and digestion of the network to form a timestep which repeats until some termination criterion is met. Note that experiments which contain contractile bonds typically have no straining phase (T_{strain}=0), so the degradation and straining happen simultaneously in the degradation phase.

analysis by checking which bonds are excluded at which timestep, as well as for positional displacement over time and analysis on the order parameter of the network.

Vertical bead displacement Vertical bead displacement is the only positional displacement that is considered. The displacement is calculated by recording the vertical position y_0 of each bead at a given timestep. Then each timestep the vertical displacement is calculated by

$$\Delta y = y - y_0, \tag{18}$$

which uses the current vertical position y. The mean of all of these displacements is taken as a quantitative indicator of the vertical movement of the entire network.
In the experiments a MMP line is created at a given vertical location y_{secrete} at a certain timestep. At this timestep the beads are divided by checking if their vertical position is above or below y_{secrete}. Their y_0 is assigned to whatever the value of y is at the timestep of division and they are then considered separately. This is to see how the position relative to the MMP and thus the removal of stresses moves the network.

Order parameter The order parameter is a measurement which is used to find the degree to which vectors are aligned. The order parameter S calculation uses the coordinates of the beads from each

bond translated to the origin as vectors $v_1, \ldots v_m$. This method, as proposed by Borthagaray *et al* [77] determines S as the largest eigenvalue of the Q-matrix

$$Q = \frac{1}{m} \sum_{i=1}^{m} 2 v_i v_i^\top - I, \tag{19}$$

which results in a value for S between 0 and 1. In the most simple case of two vectors, if both vectors are completely symmetric the order parameter is 1. Vectors that point to perfectly opposite directions, so at an angle of 180 degrees also have order parameter 1. When the vectors are at an angle of 90 degrees the order parameter is 0. This approach is chosen because bonds do have an angle, but have no polarity. This is also very similar to the approach in earlier work on image analysis of ECM collagen fibril networks [78].

Heatmaps To see how the network topology changes locally, a heatmap is used in some experiments. The network topology aspects that are mapped are the collagen bond density, the collagen bond strain and the local order parameter of the fibrils. The PDE field is divided into 20x20 bins and for each bin the bonds inside are selected for the calculations. A bond is considered inside the bin when at least one of their two beads is inside the bin region, meaning that bonds can be included in multiple bins. The density heatmap gives a quantitative indication of the location of non crosslinker bonds, since it is hard to determine and compare visually from simulation snapshots. The order parameter heatmap gives a quantitative indication of the orientation of the bonds. These heatmaps together therefore should give a good idea of the local change in topology as a result of the degradation in the different areas. A third heatmap for the average strain experienced by the bonds in each bin is used to inspect how the digestion affects the strain values in the changing topology, since they are directly influenced by the removal of stresses.

3 Results

3.1 MMPs digest the matrix locally

To test the added features for collagenase degradation by MMP in the extended CPM, first a verification of functioning was performed. This was approached using a simple threshold probability function as described in Section 2.2.2, in which the digestion probability is zero when the MMP concentration is below a threshold and one when above the threshold, instantly breaking all the bonds at the lattice space.

The goal of this first set of experiments was simply to evaluate if the mapping of the hoomd bonds to the lattice space was successful in approximating the location of the bonds without losing too much fidelity to function. Local concentrations of MMP were secreted to visually verify that the spatial mapping works. The chosen c_{th} of 0.1 is not related to any biological values.

In Figure 6, a zoomed in toy example can be seen that shows how the concentration of MMP increases at the secretion point and diffuses out, slowly digesting collagen when the concentration passes the threshold. We can confirm that MMPs can digest the fibrous matrix locally. An interesting observation to make is that the orientation of the bond to the MMP concentration matters in how quickly the threshold concentration is met. Because the concentration is averaged over all lattice spaces a bond covers, a bond that is oriented into the higher concentration at one end and outside of the concentration at the other end will experience a lower average concentration. A bond oriented more perpendicular to the concentration will more quickly experience a high average concentration. This results in the situation in Figure 6d, in which the only fibres close to the source of secretion are those that point directly towards the source of secretion.

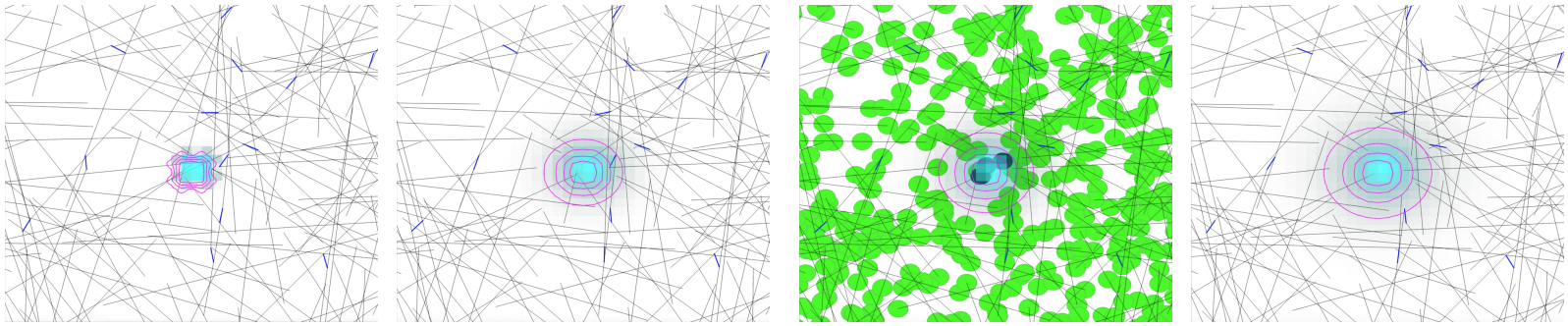

Figure 6: Progression of simulation of a small toy example of MMP secretion from a point source. The resulting diffusion and degradation happens with a threshold probability function (above a concentration value of 0.1 the probability of digestion becomes 1). Figure 6a shows the start of secretion (t=0). Figure 6b shows diffusion of the secreted MMP, start of degradation (t=5). In Figure 6c, the underlying beads are shown. Beads that have no bonds left have been deactivated and are shown as black. Figure 6d shows continued diffusion and degradation (t=10).

3.2 Collagen digestion by MMP changes network topology under stress

After confirming that local concentrations of MMP correctly digest the nearby matrix fibres, we are interested in how restructuring on a larger scale would work. To investigate this, a larger area of MMP secretion will be selected in an artificially strained network. For this simulation Δy was set to 1.5 and t_{MDstrain} was set to 200000 to increase the straining of the network and so exaggerate the effects of digestion. To ensure only the line of MMP has influence, the diffusion coefficient and secretion rate were lowered to 9.375e-13 $\mu m^2 s^{-1}$ (3e-13 in TST) and 0.09 s^{-1} (0.018 in TST) respectively. This leads to a lower diffusion length of 4.6875e-11 instead of 7.8125e-11. The same threshold function is used as described in Section 3.1, with digestion set to digest both regular collagen fibrils and crosslinkers equally. During and after straining, both the top and bottom beads are locked to be stationary and so retain the stresses applied through straining.

In Figure 7 the influence of local digestion is shown to properly interact with an entire network, where the artificially strained network is cut by a line of MMP secretion. Due to the stationary beads applying stress, the elastic properties of the collagen fibres take effect after the bonds propagating the stress in the network are digested. This causes a noticeable recoil and separation of the network, best seen in how the stretched out lower part relaxes back down into an unstrained state (see Figure 7d).

The straining of the network and subsequent relaxation after degradation of the stress bearing bonds is quantitatively illustrated in two plots shown in Figure 8. The simulation shown in Figure 7 was repeated three times and averaged to get these results.

The vertical displacement of the simulation beads (see Equation 18) over time is shown in Figure 8a. During the straining phase, the beads move upwards from their position at t=0 resulting in a positive vertical displacement. The mean displacement after straining is about 50, so a quarter of Ly. Beads higher in the space moved more because they are more close to the straining force, with the mean balanced out by beads lower in the simulation space. Note as well that the floating fibres, that is those not connected to the network by crosslinkers, contribute a displacement of about zero and so diminish the mean.

From the start of the secretion phase, there are two plots to show the difference in movement for the two partitions resulting from digestion. The plot for the beads above the secretion line continues to move upwards as the upper partition relaxes upwards. Contrary to this is the relaxation back down for the the beads below the secretion line. Note that the movement upwards is larger than the movement downwards. While the amount of beads and bonds above and below the secretion line is about equal, the lower part of the network is generally less strained and relaxation downwards results in less movement.

The shift in order parameter of the network over time is shown in Figure 8b. The order parameter is a measure of the alignment of the bonds that lies between 0 and 1 (see Equation 19 for the definition). The plot shows the order parameter between all bonds in the simulation. The expectation is that the strained network has a higher order parameter, since the network under vertical strain will force bonds to lie vertically. The plot shows that straining does increase the order parameter and the relaxation after digestion lowers it again. The order parameter does not return to the initial value while the strain levels in the network do return close to the original value. The higher ordering of the network persists after relaxation, changing this topology property permanently.

When considering that the order parameter lies between 0 and 1, the simulations did not produce a very high maximum value after the straining phase is complete. This is influenced for instance by straining not affecting the floating fibres orientation. Fibres where the bead distance between crosslinkers is higher

also seem to change orientation more than those where the crosslinkers are close on the fibre (as can be seen in for instance Figure 7b).

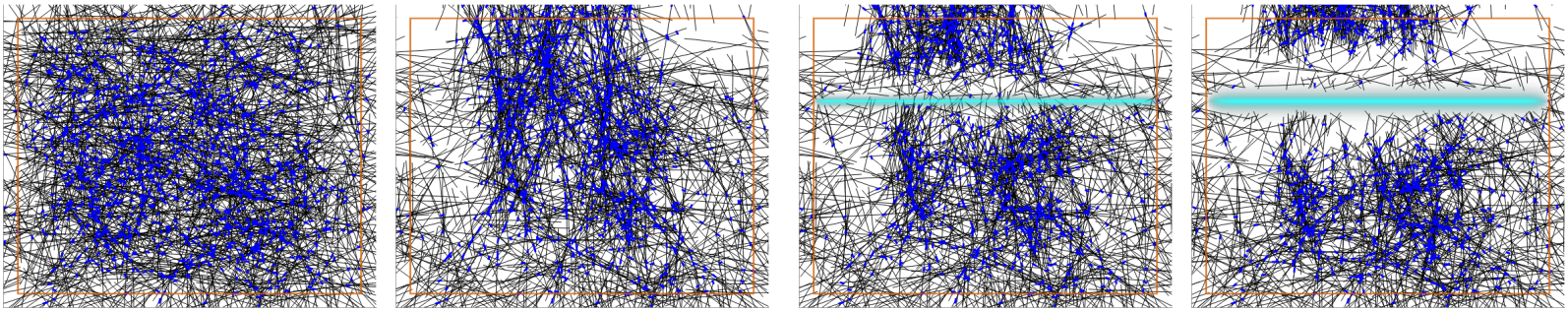

(a) **(b)** **(c)** **(d)**

Figure 7: Progression of simulation of a line of MMP digesting the collagen network with a threshold probability function (above a concentration value of 0.1 the probability of digestion becomes 1). Figure 7a shows the initial random network (t=0). Figure 7b shows the network after application of artificial strain on the upper quarter of the network, pulling it upwards (t=166). Figure 7c shows the start of secretion of MMP after straining, with the network noticeably recoiling after the bonds propagating the stress of the strain are digested and removed (t=180). Figure 7d shows the network after it has had time to relax (t=220).

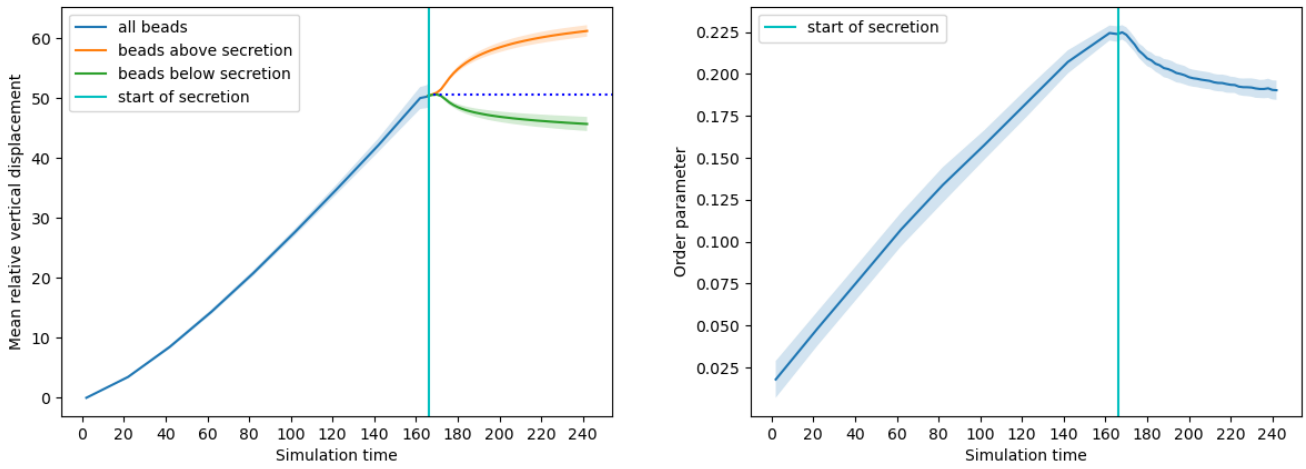

(a) **(b)**

Figure 8: Two plots of quantitative properties of the network over time. The analyses are from simulations such as in Figure 7, repeated three times and averaged. The shaded area is the standard deviation. For Figure 8a the mean vertical displacement is shown. To illustrate the network relaxing into two partitions after getting split by the line of MMP, the beads above and below the secretion line are plotted separately after secretion with the dotted line showing the position before secretion for reference. For Figure 8b, the order parameter of the entire network is calculated and plotted. Straining the network increases the order parameter and the relaxation after digestion lowers it again.

3.3 Crosslinker digestion by MMP changes network topology under stress

The digestion of collagen and crosslinkers by local concentrations of MMP has been shown to work on an entire network and cause dynamic reactions due to sudden removal of stresses. Next, we will study the effect of digestion of only crosslinkers, leaving regular collagen bonds intact. Since crosslinkers connect the individual collagen strands to actually form the network, a hypothesis to be brought up is that the stresses caused by the artificial straining propagate only through the crosslinkers. In order to see if this hypothesis is true, the same experiment as in Section 3.2 is repeated, but with the excluder module considering only crosslinkers. This means in a biological sense that the MMP specifically targets crosslinkers for digestion, but does not degrade regular collagen fibrils.

Figure 9 shows a similar change in topology as previously with both crosslinker and fibril digestion. While the network does eventually get separated due to digestion of key crosslinkers, this process takes significantly longer because the location of the stress bearing crosslinkers were not always close to the MMP concentration. To illustrate this, the timestamp of the final snapshot showing relaxation after separation in Figure 9d is later than the relaxation snapshot in Figure 7d. In most simulations there were some fibrils that still spanned the distance between the bottom partition and the top partition, because the crosslinkers connecting them to the different partitions were outside of the MMP concentration range.

Similarly to the previous section, a quantitative analysis of vertical bead displacement and the order parameter have been done (see Figure 10). These results are from three simulations such as the one presented in Figure 9, which were averaged. In Figure 10a, the vertical displacement is shown. Like previously, the displacement after the straining phase is about 50. After digestion, the beads above the secretion line move upwards due to relaxation. The beads under the secretion line move downwards. The figure also contains the vertical displacement after secretion of the previous section in grey. This illustrates that the magnitude of movement after digestion of only crosslinkers is notably smaller and slower than when digesting all bonds. Movement of beads is less when there are more stress bearing bonds remaining in the simulation. With digestion of only crosslinkers less bonds are digested in general, leaving more stress bearing bonds.

In Figure 10b, the order parameter over time is shown. During the straining phase, the order parameter rises as the network stretches out and the bonds align more. After secretion starts and crosslinkers are digested, fibres with large stresses bounce back and the order parameter lowers. Since the network does not partition fully and the remaining fibres are still oriented vertically, the order parameter stays higher than when the network would separate cleanly. Similarly to the vertical displacement, the process is also slower with an almost linear plot instead of a curve with a steep beginning.

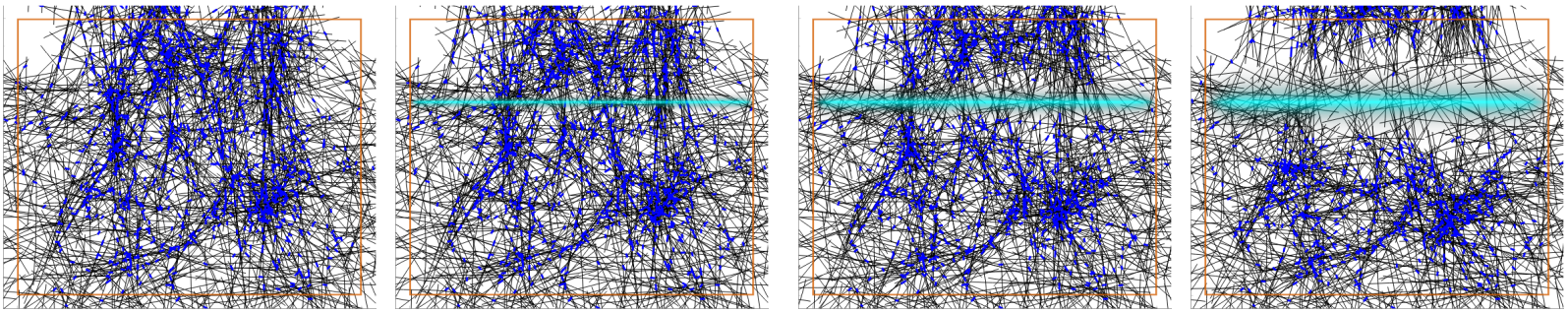

(a) **(b)** **(c)** **(d)**

Figure 9: Progression of simulation of a line of MMP digesting the crosslinkers in the network with a threshold probability function (above a concentration value of 0.1 the probability of digestion becomes 1). Figure 9a shows the network after application of artifical strain on the upper quarter of the network, pulling it upwards (t=166). Figure 9b shows the start of secretion of MMP after straining (t=180). Figure 9c shows the timestep at which simulations digesting both fibrils and crosslinkers would be separated in a relaxed state (t=200). This process is generally slower in these simulations. Figure 9d shows the network relaxed after semi-separation (t=240). The network strain values in most simulations stay higher than the strain values in the simulations with full digestion of both crosslinkers and collagen due to not all stretched fibrils breaking and recoiling.

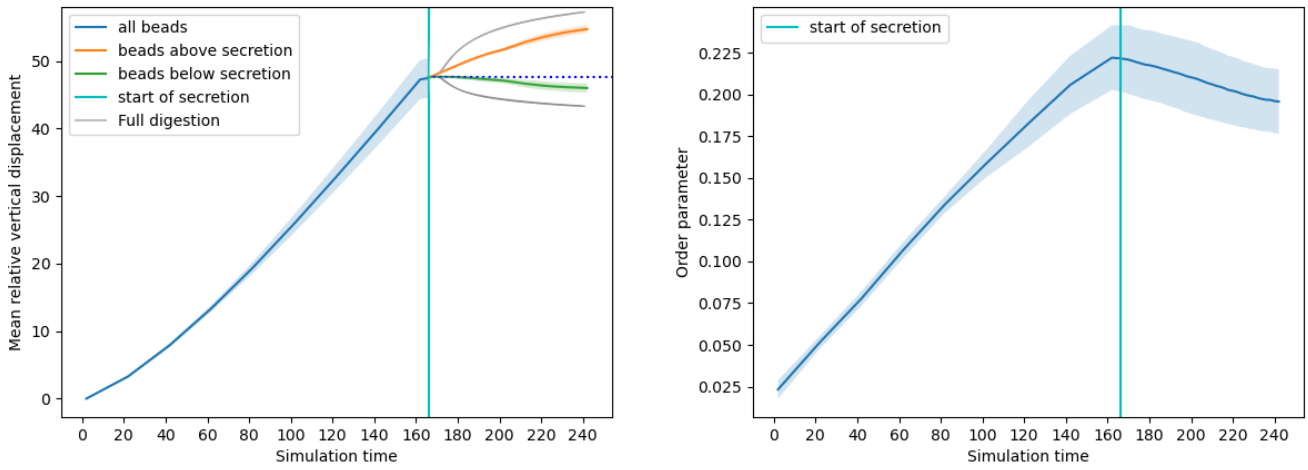

(a) **(b)**

Figure 10: Two plots of quantitative properties of the network over time. The analyses are from simulations such as in Figure 9, repeated three times and averaged. The shaded area is the standard deviation. For Figure 10a the mean vertical displacement is shown. To illustrate the network relaxing into two partitions after getting split by the line of MMP, the beads above and below the secretion line are plotted separately after secretion with the dotted line showing the position before secretion for reference. In grey, the separation of the partitions in the case of full digestion (Figure 8a) is plotted for comparison. For Figure 10b, the order parameter of the entire network is calculated and plotted. Straining the network increases the order parameter and the relaxation after digestion lowers it again, but less than in the previous experiments.

3.4 Local MMP digestion impact depends on collagen density

From the previously described experiments it has been made clear that the network can be effectively degraded by MMP concentrations, but that the location of MMP is vital to the change in topology of the network after degradation. To investigate the difference and magnitude of the effect of the location, a set of simulations was done with a set seed for the network initialization to ensure an identical network each time. These use the threshold function of Section 3.1. First a simulation without any secretion was done to set a baseline for comparison. In this simulation T_{strain} is set to 150 to exaggerate the effect of digestion. The simulation was then repeated twice, once with secretion in the low density region and once with secretion in the high density region. To create a large enough hole to impact the network topology, the diffusion coefficient D was changed to 1.5781e-13 $\mu m^2 s^{-1}$ (5.05e-13 in TST). A comparison of the effect of lower D values resulting in smaller holes can be seen in Appendix A.

Heatmaps for different aspects of the network topology (see Section 2.3.6) are used together with snapshots of the simulations themselves to inspect how the network topology changes. The first run without MMP are in the two leftmost columns in Figure 11, one showing the network directly after the straining phase and one showing the network after prolonged relaxation. In the second row, Figures 11e and 11f show that there is a distinct region of high collagen density on the right, with a lower density region on the left. In the fourth row, we observe in Figures 11i and 11j that the strains on the lower density region bonds is significantly higher than in the high density region. This is probably because a similar stress load is divided over less fibrils, thus straining them more.

The simulations with the two secretion points are in the two rightmost columns in Figure 11. It is evident from Figures 11k and 11l that the digestion of the stress bearing bonds causes the strain of the connected adjacent network to be almost entirely be eliminated. Even though there are less bonds affecting the network, the strains are much higher in the low density region prior to secretion. This causes the effect of digestion to recoil mostly upwards with a higher velocity and thus impact than in the high density region, where the recoil is much slower and goes both ways.

The density heatmaps in Figures 11g and 11h show that the general region above and right of the low density zone becomes more dense. For the high density region, only the directly adjacent regions above and below show a change in density.

The local order parameters are compared in Figures 11o and 11p. The order parameter directly around the MMP fields should be taken with a grain of salt, since there are very few bonds left in the area and so the alignment is generally higher. With this in mind, we do not see a large change in the local order parameters. The largest changes observable are the lower order parameter below- and the higher order parameter above the low density secretion field. The high density digestion simulation shows a similar pattern with lower parameters below and higher parameters above, but of a lower magnitude.

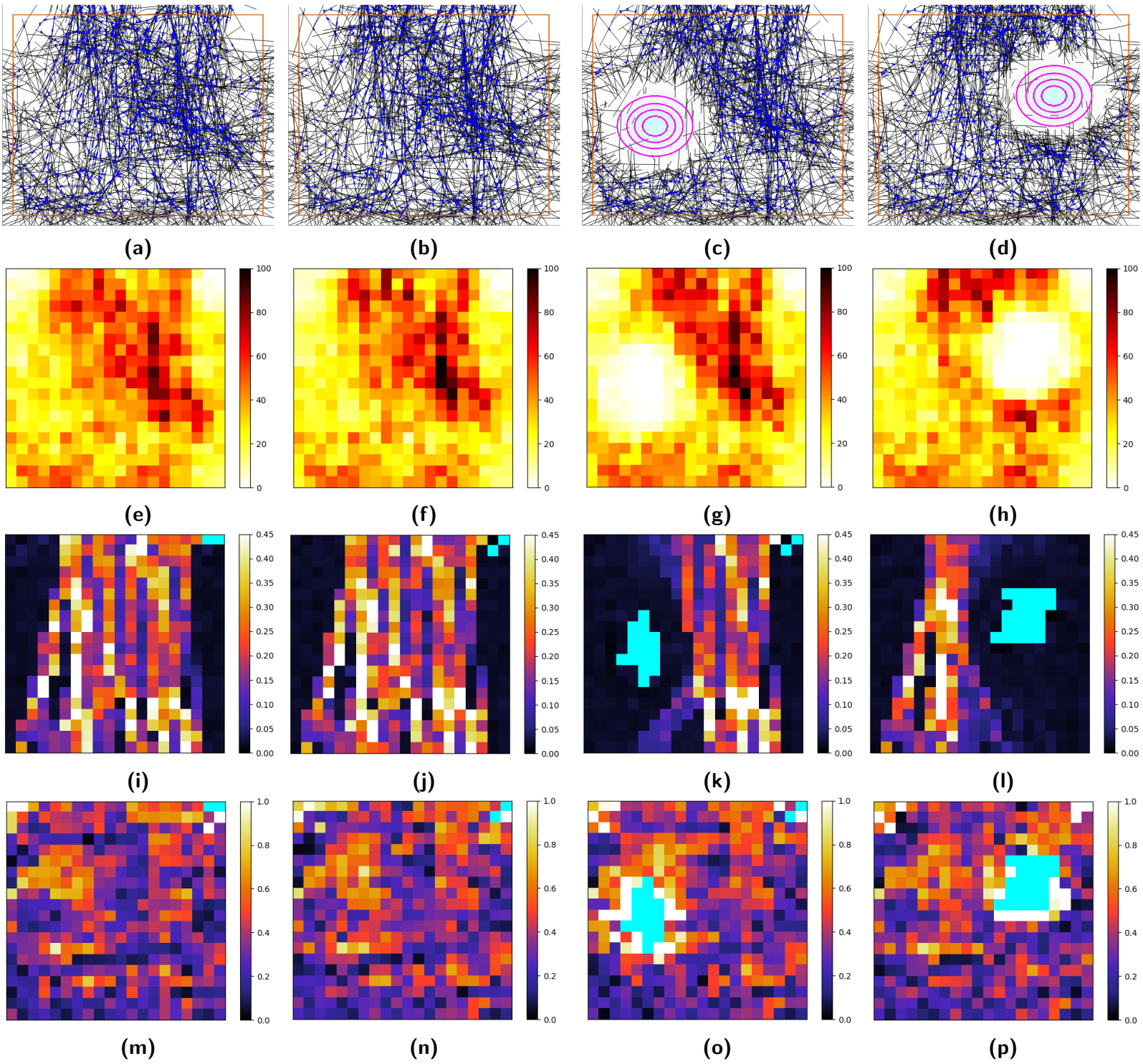

Figure 11: Comparison of the effect of two secretion locations, one in a low bond density area and one in a high bond density area. Each column of figures represents the same snapshot. Figures 11a to 11d show the snapshots of the simulations. Figures 11a and 11b show a simulation without any MMP as a baseline (t=155 and t=271 respectively). In Figures 11c and 11d a manually selected low density area and high density area respectively are digested by secretion of MMP (t=271 for both). Figures 11e to 11h show regular collagen bond density heatmaps of the snapshots, with the PDE field binned into 20x20 bins. A bond is included in a bin when at least one bead of the bond is inside the bin. Figures 11i to 11l show the mean strain for the same bins and Figures 11m to 11p show the local order parameter in each bin.

3.5 Strained bonds survive longer while subject to collagenase

Next we test the model in presence of strain protection (see Section 1.3 for the relation between strain and collagenase degradation rates). This qualitative result has been quantified many times and generalized into degradation laws (see Section 1.4.1). In order to see if the model also shows the qualitative behaviour of strained fibrils surviving far longer than unstrained fibrils as seen *in vitro*, a set of simulations was run using the simpler Loerakker degradation law 1. This law determines a sigmoid function from a maximum degradation rate at lower strain values, to a minimum degradation rate at higher strain values. The Loerakker degradation laws are subject to parameters. These parameters are listed in Parameter Table 1, but of interest here are Ξ_{max} and Ξ_{min}. For these simulations, to get a good first idea of the qualitative results, $\Xi_{\text{max}} = 1.0$ and $\Xi_{\text{min}} = 0.0$. These settings are exactly the same as in Figure 3a.

In these simulations, a network is subjected to artificial strain as in the previous experiments. After straining, a uniform field of MMP is applied to the simulation space. This setup is very similar to some of the experiments *in vitro*, in which an established collagen network is strained with pipettes or attached springs, after which a uniform solution of collagenases is dropped onto the dish, affecting the entire network simultaneously [46–48].

From the simulations, it becomes clear that replacing the threshold function in the degradation algorithm with the Loerakker degradation law 1 will cause the model to protect strained collagen (see Figures 12a to 12d). Since the degradation rates of strained collagen become $\Xi_{\text{min}} = 0.0$, eventually the strained bonds will be the only ones remaining. All other less strained bonds have higher degradation rates and will thus sooner or later be digested. Compare this with Figure 2, an experiment *in vitro* with a very similar qualitative result as the *in silico* model simulations. In the experiment presented in the figure only the fibrils that were strained by the pipettes remain, while surrounding "peripheral" fibrils are digested. While not exactly identical due to the different physical scale, time scale and the method for artificial strain, the model also clearly has only strained collagen remaining at the end of the simulation.

To see how much the strain applied to the network influences the protection of fibres, two control groups with lower strain rates were simulated as well. In these simulations, the parameter influencing how much vertical displacement to the top beads is applied each step in the pulling phase Δy was changed to 0.0 and 0.5. Figures 12e to 12g show a qualitative comparison of control simulations to a simulation with $\Delta y = 1.0$. In Figure 12h, the average count for three repetitions of such simulations is presented. In these counts it is clear that a lower strain rate causes less fibres to be strained to a value high enough to be protected from degradation.

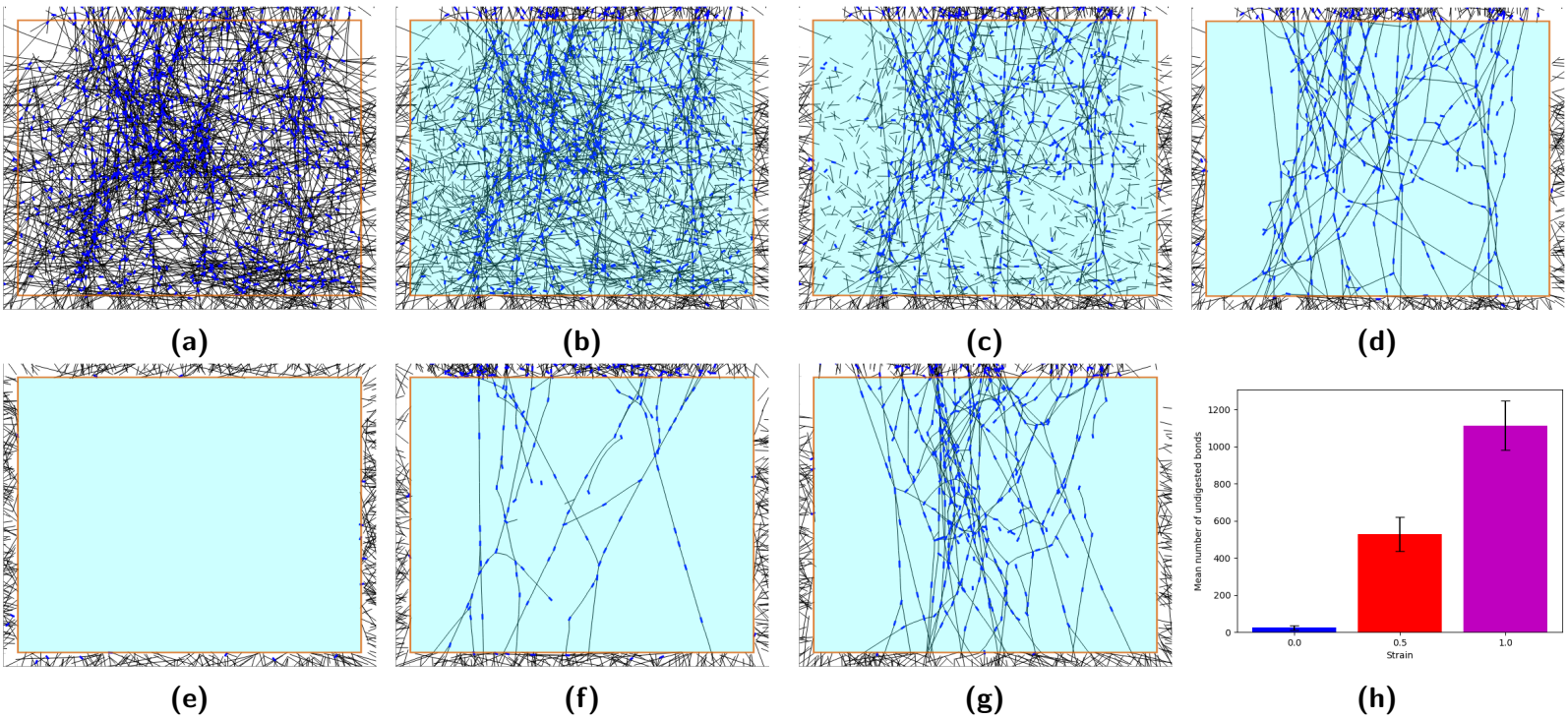

Figure 12: Figures 12a to 12d: Snapshots of progression of a simulation, in which a homogeneous concentration of MMP is instantaneously applied to a strained network. In this simulation Loerakker degradation law 1 is used, with a Ξ_{max} of 1.0 and a Ξ_{min} of 0.0 (see Figure 3a). Figure 12a shows the network after application of artificial strain (t=86). Figure 12b shows the instantaneous addition of a homogeneous MMP concentration (t=88). Bonds with little to no strain have a high degradation rate and are removed quickly. Bonds with a high enough strain have a degradation rate of (close to) zero. In Figure 12c one can already visually distinguish the bonds with a higher strain, since they continue to form a network with each other, while lower strain strands detach from the network and float (t=91). In Figure 12d, only the high strain bonds remain after a longer simulation time (t=116). Note the similarity of Figure 12d to Figure 2. The global order parameter values for the snapshots are 0.0321, 0.1640, 0.1961 and 0.2360 from left to right. This shows that the remaining strained network has a higher ordering when the unstrained bonds are filtered out over time.
Figures 12e to 12h: Snapshots at the end of the simulation (t=166) for different displacements ($\Delta y = 0$, 0.5, 1) per puller module call, with a mean count and standard deviation bar (3x repeated) of undigested bonds at this time shown in Figure 12h. This comparison shows that the value of Δy influences the strain values in the network and thus indirectly the digestion rates resulting in different numbers of protected and digested bonds with $\Xi_{\text{min}} = 0.0$.

3.6 The choice of degradation law has minimal effect

As shown in the previous section, implementing Loerakkers first degradation law with $\Xi_{\text{min}} = 0.0$ yields the same qualitative results as *in vitro* experiments. Next we will compare the difference between the first and second degradation law created by Loerakker *et al*. This second degradation law can be seen in Figure 3b and models both a decrease in degradation rate when the strain increases as well as an increase in degradation rate when strain becomes too high. Interestingly, in the paper in which the degradation laws were presented, there was no functional difference between the laws in the experiments they performed. This was reported to be due to the strain values in their model simulations never exceeding the strain values at which the degradation rate increased again.

To investigate if changing to Loerakker degradation law 2 does yield significant different results to degradation law 1 in our model, simulations with both laws were repeated 5 times, still keeping $\Xi_{\text{min}} = 0.0$. The comparison can be seen in Figure 13. As can be seen, qualitatively both laws perform identically since there is no distinction to be made between the top row and bottom row of snapshots. When looking at the quantitative analysis in Figure 14, the laws perform very similarly. Generally, the simulations with Loerakker degradation law 2 have less bonds surviving at the end, since the few bonds with a too high strain are digested, but the difference is minimal.

This outcome is similar to what Loerakker *et al.* observed after implementing both laws. Because the strain values for most bonds in the simulation do not exceed the strain value at which the degradation rises again, the simulation behaves largely the same for both laws. Additionally, bonds that do exceed the minimum degradation strain value exceed the point only by a little bit.

Disregarding the random initialization, all simulations went through the same process in the same timeframe and it seems that for the parameter values studied the choice of degradation law has no effect. Additionally, this lack of difference is not subject to parameters Ξ_{max} and Ξ_{min}, since they only influence the degradation speed at a given strain. A lower Ξ_{max} for instance, would reduce the degradation rate for simulations with both degradation law 1 and degradation law 2 equally. Relatively to each other the degradation rates stay the same so the similarity will hold. Due to this, all following experiments will be conducted with the simpler Loerakker degradation law 1. It has to be noted however, that it is possible that these results of similarity are due to the specific strain rate and straining duration of the simulations. Due to the nature of bulk mechanics and the distribution of stress through the network, maybe a larger stretching of the network would result in noticeable qualitative differences. Still, like the Loerakker situation, there is little functional difference between the laws.

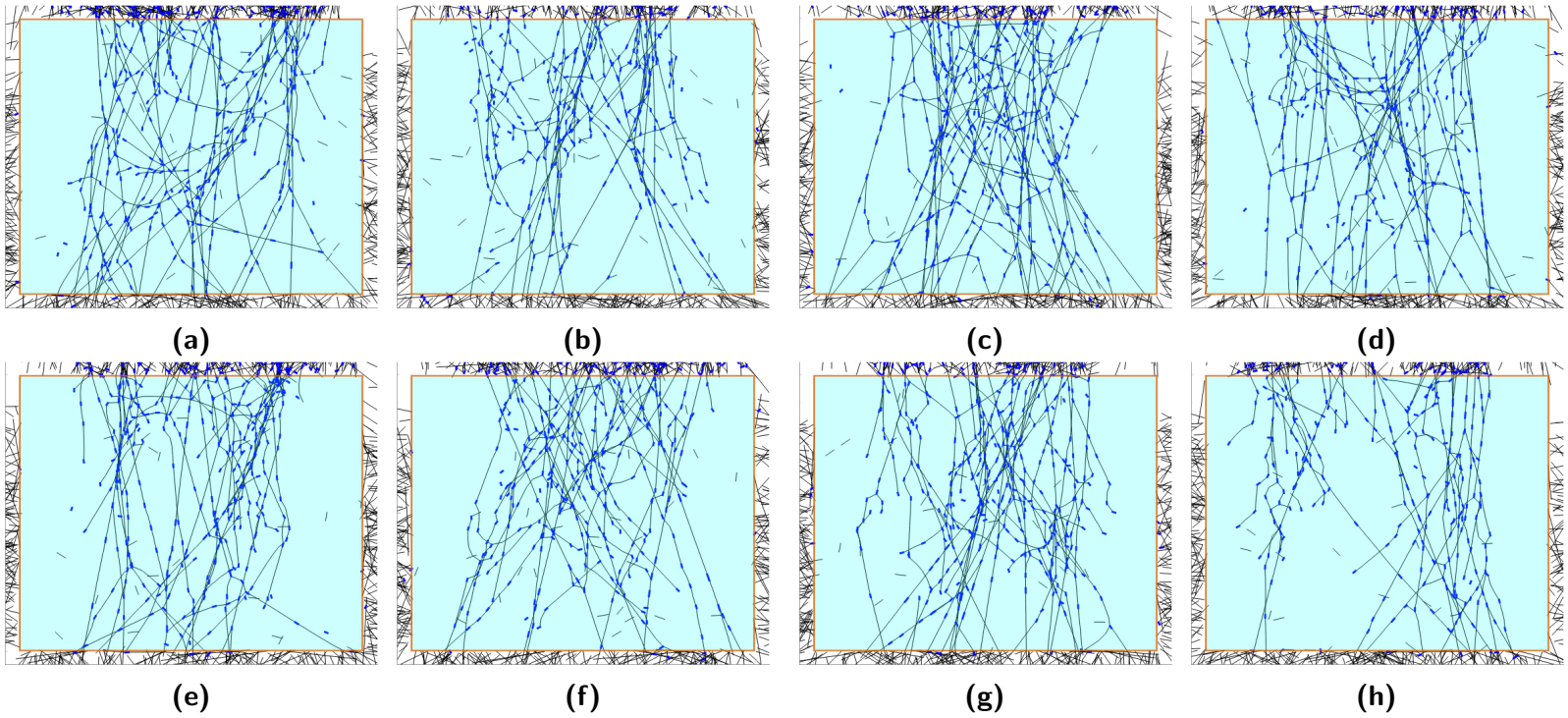

Figure 13: Snapshots of the same timestep (t=116) of simulations with Loerakker degradation law 1 in the top row (Figures 13a to 13d) and Loerakker degradation law 2 in the bottom row (Figures 13e to 13h). Qualitatively, the results are indistinguishable when disregarding the random network the simulations started in. All simulations end up with a protected strained network remaining after digestion of unstrained (and for law 2, overstrained) bonds. For comparison, the mean global order parameter for the top row is 0.2276 and the mean global order parameter for the bottom row is 0.2453, so also very similar.

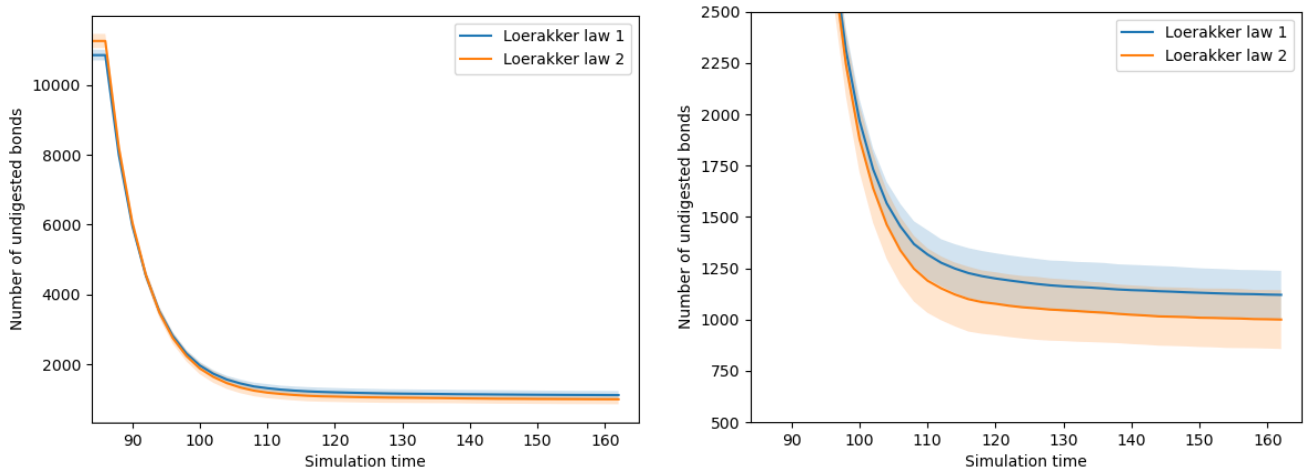

Figure 14: Plots illustrating the minimal difference of Loerakker degradation law on the degradation rate and number of remaining bonds. Figure 14b is a zoomed in view of the same plot in Figure 14a. This quantitative analysis is of the same simulations seen in Figure 13, averaged. The shaded area is the standard deviation.

3.7 The value of Ξ_{min} influences digestion rates

Thus far, the experiments have used $\Xi_{max} = 1.0$ and $\Xi_{min} = 0.0$ as parameters for the Loerakker degradation laws. In the paper introducing the laws, Ξ_{min} is set to 0.5 instead. In their model, Loerakker *et al.* modeled collagen in a very different way, in a different context and also taking into account collagen production laws to counteract the degradation. This means that a Ξ_{min} of 0.5 does not translate to the model discussed here. $\Xi_{min} = 0.0$ is a safe place to start, since it is easier to verify the functioning of the model when the lowest degradation rate is no degradation at all. *In vitro* experiments have shown however, that even strained fibrils will eventually get digested by collagenase.

A set of experiments was carried out with Loerakker law 1 to find which values of Ξ_{min} would reasonably yield a qualitative result similar to the *in vitro* setting. From these experiments it was quickly discovered that values $\Xi_{min} \geq 0.1$ would result in an quickly emptied simulation space. The set of simulations for a range of values $0.01 \leq \Xi_{min} \leq 0.09$ is shown in Figure 16. The higher Ξ_{min}, the harder the qualitative result becomes to discern. In the figure, the difference between $\Xi_{min} = 0.01$ and $\Xi_{min} = 0.09$ is obvious, but there seems to be a change of behaviour from distinct strained fibril networks remaining between floating loose bonds to no discernible visual difference between the strained and unstrained bonds after the initial artificial straining of the network.

Because the difference is hard to see visually, a quantitative analysis of the number of digested bonds over time was done for each shown Ξ_{min} setting in Figure 16 plus the original $\Xi_{min} = 0.0$ setting. The plot of this analysis is presented in Figure 15. The total number of digested bonds and the degradation rate is clearly distinguishable for the lower Ξ_{min} values, but for $\Xi_{min} \geq 0.03$ the difference seems to be mostly dependent on the random initialization and the randomness used in the degradation algorithm.

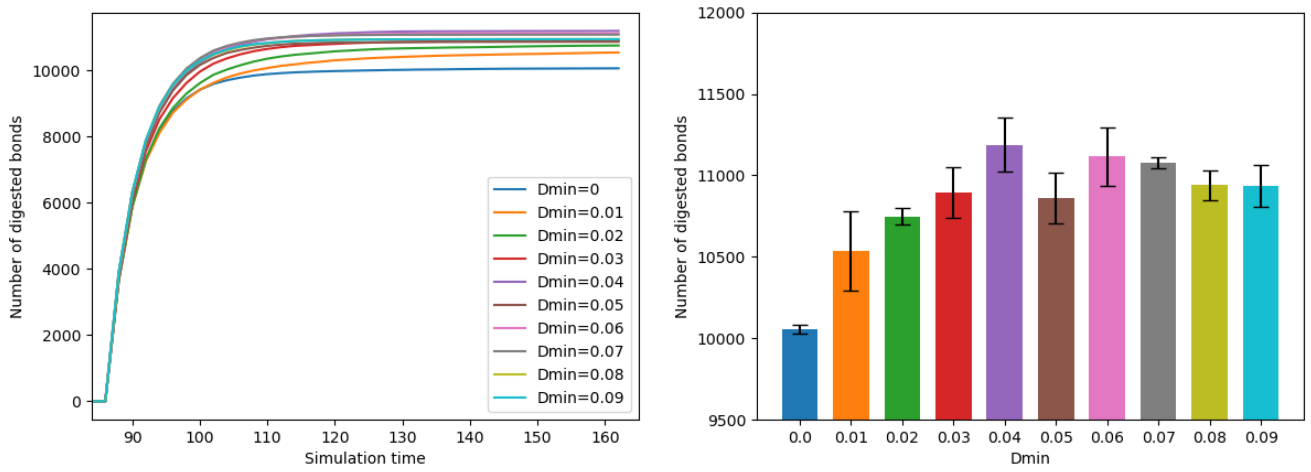

(a) **(b)**

Figure 15: Plots illustrating the effect of the Ξ_{min} parameter in Loerakker degradation law 1 on the degradation rate and number of digested bonds. Figure 15a shows a plot of the number of digested bonds over time for different Ξ_{min}. Figure 15b shows a bar plot with standard deviations of the last timestep of the plot in Figure 15a. This quantitative analysis is of the same simulations seen in Figure 16, repeated three times and averaged.

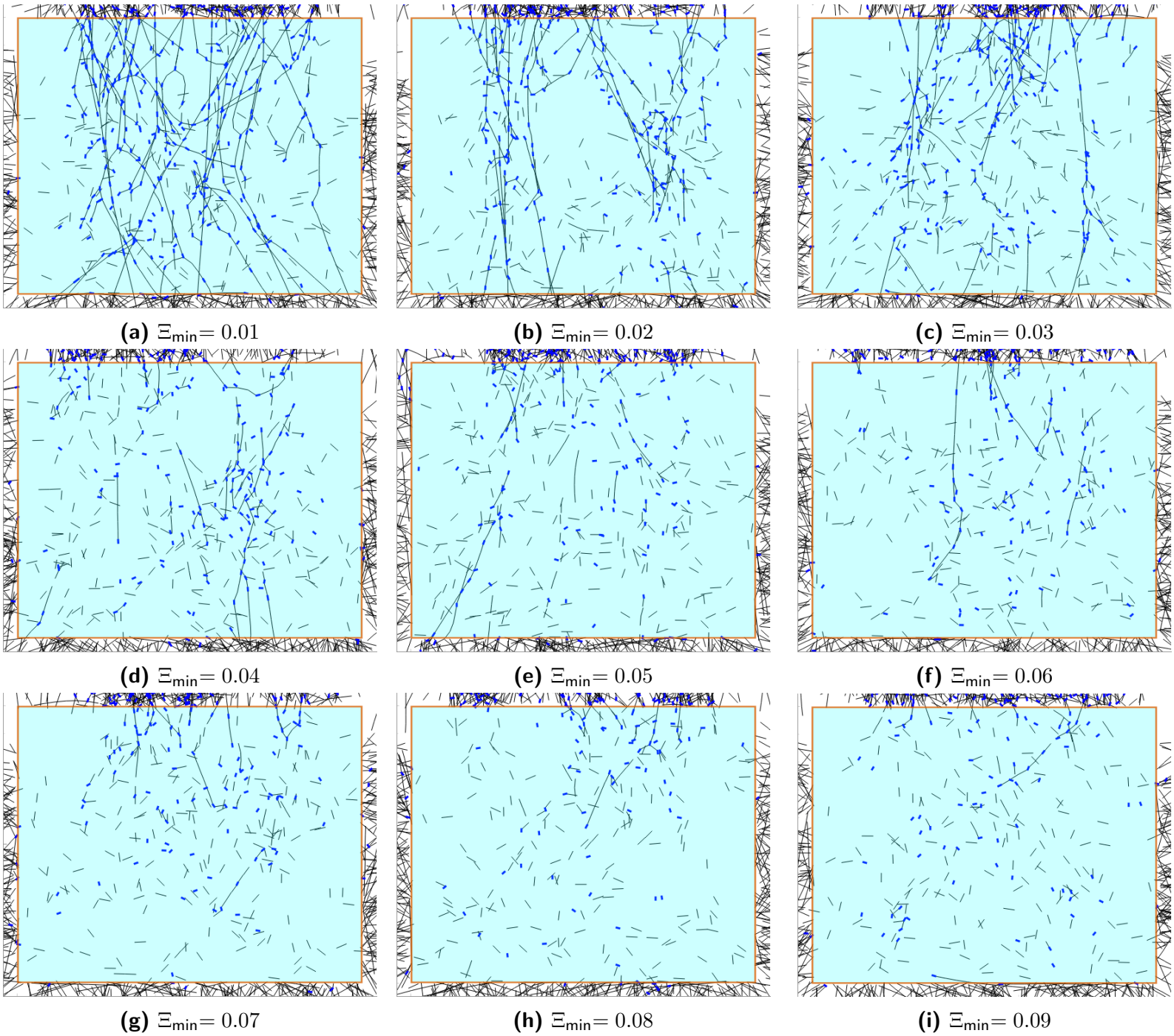

(a) $\Xi_{\text{min}} = 0.01$ **(b)** $\Xi_{\text{min}} = 0.02$ **(c)** $\Xi_{\text{min}} = 0.03$

(d) $\Xi_{\text{min}} = 0.04$ **(e)** $\Xi_{\text{min}} = 0.05$ **(f)** $\Xi_{\text{min}} = 0.06$

(g) $\Xi_{\text{min}} = 0.07$ **(h)** $\Xi_{\text{min}} = 0.08$ **(i)** $\Xi_{\text{min}} = 0.09$

Figure 16: Snapshots of the same timestep (t=150) of simulations with different values for Loerakker degradation law Ξ_{min}, ranging from 0.01 to 0.09. The range of Ξ_{min} values shows a spectrum of results; the higher Ξ_{min}, the less the qualitative result of strained bonds surviving longer can be seen. At some point, it becomes impossible to distinguish the strained bonds from the unstrained, since they all degrade very quickly.

3.8 The concentration of MMP affects degradation rate

After investigating the effects of varying Ξ_{min}, one might expect a similar investigation on Ξ_{max}. Instead of directly changing this value however, the concentration of the MMP in the simulations will be varied. In the previously described simulations, the assumption is made that the entire simulation space contains a uniform concentration of MMP. In the *in vitro* experiments, this might be the case, but *in vivo* MMP is locally secreted by cells and diffuses, so the concentration is not uniform. The *in vitro* experiments for the effect of strain on collagenase degradation rate have been performed with different concentrations, so we know that the phenomenon of strain protecting collagen is not dependent on a specific MMP concentration. In Section 1.3 it is explained that we know that the relation between concentration and degradation rate is linear, but no specific Michaelis constant and slope can be determined to be used in the simulations, due to the variety of exact values reported. Thus a simplification is made to allow for concentration to influence the degradation rate.

In the following simulations, the concentration of MMP is bounded $[0, 1]$. This is to be interpreted as $0 - 100\%$ of the concentration used to determine the strain-degradation rate relation. We use the concentration value as a multiplier to the degradation rate, effectively letting the MMP concentration influence the degradation rate linearly. To see if this approach functions as expected, a vertically strained network such as in the previous simulations was subjected to a concentration gradient between 0 and 1 (with diffusion turned off).

Both a horizontal gradient and a vertical gradient were simulated and in Figure 17 the effect of the gradient is clearly visible. While strained bonds will always survive, the digestion of unstrained bonds is subject to the concentration gradient. This means the desired effect is reached, successfully abstracting the Michaelis-Menten kinetics relation between collagenase concentration and collagen degradation rate.

To get an indication on the quantitative effect of the concentration gradient, a measurement of lifetime was used. The time at which a bond is digested is used for this measure, recording the amount of simulation time elapsed after application of the MMP concentration. For each bond, the location of one of its beads is used as its approximate position. The positions in the 200 x 200 PDE field are binned into 200 bins horizontally and 200 bins vertically. For each bin the mean lifetime is taken. This lifetime-spatial distribution relation is plotted in Figures 17d and 17h. While there is local variation, the general trend of a longer lifetime for higher concentration is apparent. The remaining bonds at the end of the simulations are not accounted for in the plot, since only degradation time was recorded. Note as well that values near the bounds of the PDE field might have slightly inflated numbers for bonds that exist partially inside and partially outside of the concentration, since they experience less MMP and thus survive longer.

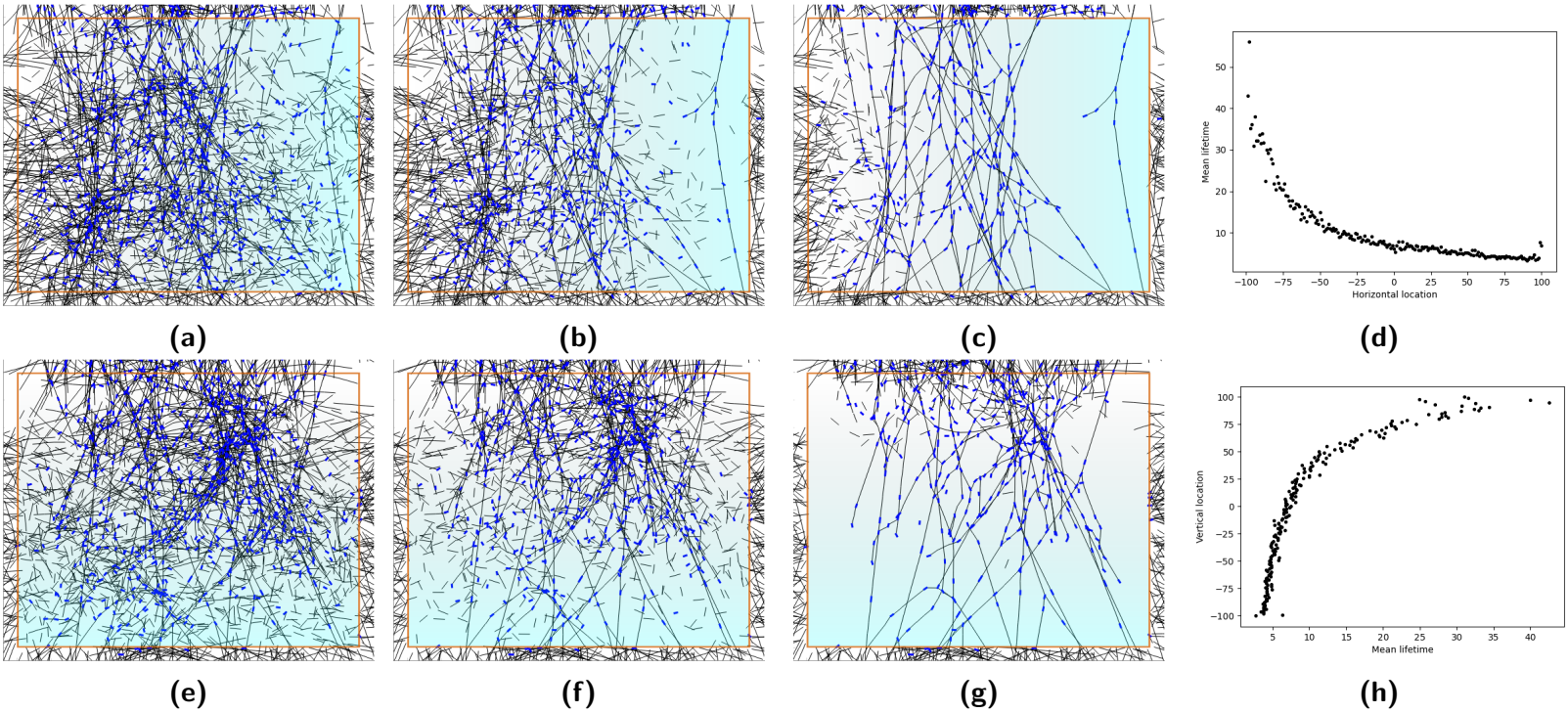

Figure 17: Snapshots of two simulations, in which a gradient concentration of MMP is instantaneously applied to a strained network. The upper row shows a horizontal gradient and the lower row shows a vertical gradient. In these simulations Loerakker degradation law 1 is used, with a Ξ_{max} of 1.0 and a Ξ_{min} of 0.0 (see Figure 3). Figures 17a and 17e show the immediate effect of the addition of the horizontal and vertical MMP gradients (t=91). Figures 17b and 17f show that in the high concentration areas on the right and bottom the unstrained bonds are quickly digested (t=96). In the medium concentration in the center the strained bonds become distinguishable. Figures 17c and 17g show that even after letting the simulation run for longer the unstrained bonds in the left and top low concentration areas remain (t=126). The mean time of digestion after secretion of MMP is plotted in Figures 17d and 17h for each bond based on its horizontal or vertical location (repeated three times, averaged).

3.9 Cellular contractile forces locally protect collagen against MMP digestion

After the previous experiments investigated the effect of specific relevant parameter settings in an artificial setup, the experiments in the following two sections aim to apply the gathered knowledge from the results about the functioning of the model to a scenario more akin to *in vivo* cell behaviour. The simulations aim to mimic the behaviour of cells reshaping the ECM through simultaneous application of contractile forces to the adjacent collagen network and secretion of MMP. This means that there is no more strain phase to set up a prestrained network (T_{strain}=0), since we want to see the emergent dynamics between a developing local MMP concentration field and a network in the process of getting strained.

The experiments will combine strain protection and concentration scaling with a MMP gradient caused by secretion and diffusion. The simulation will not explicitly model a cell, but will model the effects a cell would have. It will make use of the contractile bond generation at the start of the simulation to mimic a cell contracting (see Section 2.3.1) and use a circular secretion to mimic the secretion of MMP by a cell (see Section 2.3.2). Figure 18 shows an overview of the resulting model behaviour from this setup. Each column represents a progression in time, with the upper row showing snapshots of one of the simulations. The same network property heatmaps as in Section 3.4 are used to quantify the progression. Each heatmap shows the mean values of three simulations. Some simulations lack bonds for certain bins, so there is no strain or order parameter to calculate. These bins were ignored in the mean calculation (referred to as a NaN mean).

The contractile force applied to the beads moves them towards the center, which strains the bonds attached to the beads. Due to their length becoming longer than the resting length, they pull on the beads on the other side of the bond. This effect cascades through the network, straining bonds closer to the center more than bonds further away from the center. While the contractile force application and secretion proceed at the same time, the straining of the bonds happens fast enough to ensure the bonds adjacent to the selected contractile beads are protected from digestion. Quickly a divide becomes clear, with a high density center surrounded by a "moat" of MMP concentration. Over this moat, only strained fibril bridges remain between the center and the surrounding unstrained network.

The MMP also secretes inwards, pruning the outside of the center as well as digesting the unstrained network. Exploratory experiments with different secretion radii indicate that the size of the secretion circle influences mainly the size of the center cluster, but the rest of the simulation proceeds the same (see Appendix B for an exploration of this).

The order parameter heatmaps show well that a randomly generated network with a low order parameter can locally be manipulated into a highly structured pattern through application of contractile forces and secretion of MMP.

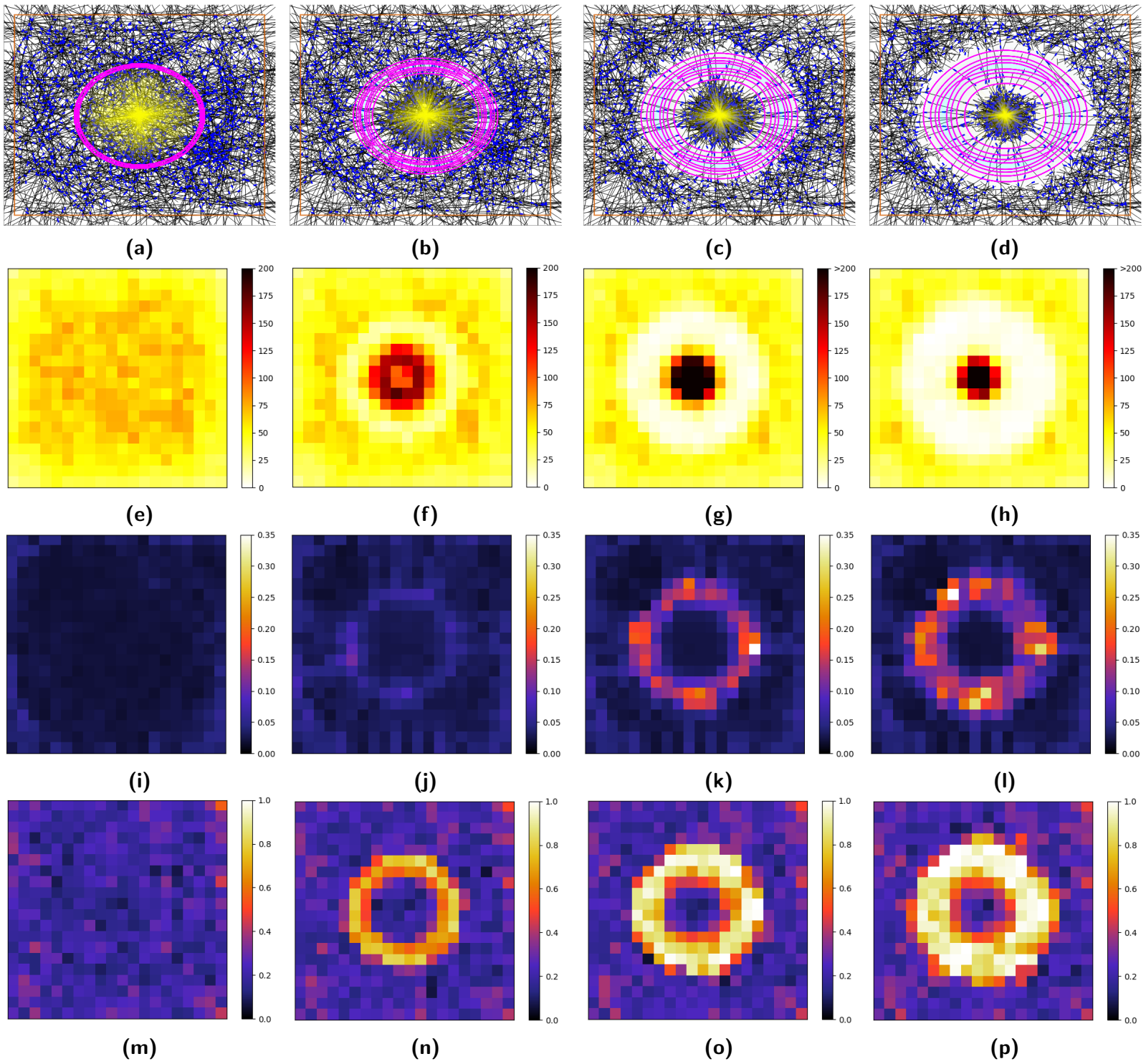

Figure 18: Progression of simulations with a central contractile force applying artificial strain and simultaneous strain based concentration dependent degradation by MMPs secreted in a ring around the center. Each column of figures represents the same snapshot (t=0, t=86, t=186, t=260 from left to right). Figures 18a to 18d show snapshots of an example of such a simulation. Figures 18e to 18p show heatmaps of network properties, with the PDE field binned into 20x20 bins. A bond is included in a bin when at least one bead of the bond is inside the bin. The heatmaps contain mean values of three simulations. Figures 18e to 18h show heatmaps of collagen density. Figures 18i to 18l show heatmaps of the strain values and Figures 18m to 18p show heatmaps of the local order parameter.

3.10 The amount of contractile force affects local collagen protection

The previous section shows that contractile cellular forces protect local collagen of MMP degradation through strain, but concedes that the way the contractile force is created is not entirely alike to how cells actually apply this force. One change that would bring the model more towards the *in vivo* scenario is lowering the amount of beads selected for contractile bond creation. Cells connect to the ECM by creating focal adhesions [79] around the edge of the cell similar to the previous setup, but they do not create focal adhesions with every single possible connection point. The process of focal adhesion creation is a complex one and is dependent on a number of factors, such as ECM properties. Here this process will not be incorporated, but a drastically lower number of focal adhesions will be selected. In the previous section the model created between about 2500 and 3000 contractile bonds (depending on local density created by the random initialization). For the following experiments this will be lowered to 100 contractile bonds, with a random selection of which beads in the selection radius receive a contractile bond.

Lowering the number of contractile bonds while keeping the spring constant the same per bond will result in a lower total contractile force applied by the cell. Determining a reasonable balance between the number of contractile bonds and the spring constant of those bonds to ensure protection similar to the baseline set by the previous sections experiments opens up an interesting comparison to previous work. In the paper in which the original model is introduced, the interaction of a contracting cell connected to the ECM using a similar number of focal adhesions is investigated [63]. One of these aspects of the interaction is the displacement caused by the contracting cell, which is a direct consequence of the balance between the contractile force and the elastic force of the ECM pulling back. One of the major parameters changing this dynamic in the paper is the crosslinker density, which governs the network stiffness. Instead, here the other side of this dynamic will be investigated by varying the level of contractile force instead of the stiffness of the network. Simulations with a range of values for k_{ct} increasing from 0.1 to 1.0 were performed, with each k_{ct} value simulation repeated three times, to see which value of k_{ct} provides which amount of collagen protection through strain at the given number of 100 focal adhesions.

Similarly to the previous experiments with a range of Ξ_{min} values, the difference between for instance $k_{ct} = 0.1$, $k_{ct} = 0.5$ and $k_{ct} = 1.0$ is qualitatively clear (Figures 19b to 19d), but the intermediate steps do not seem to differ much. Additionally, quantifying the effect of k_{ct} for the higher values of k_{ct} is difficult. Figure 19a shows the mean number of digested bonds for each value of k_{ct}, in which a clear general downtrend implies that a higher k_{ct} leads to less digested (ergo more protected) bonds. However, it does not always hold that less digested bonds also implies more protected bonds. Note for instance that the standard deviation bars grow larger as k_{ct} goes up. This trend is also true for larger values of k_{ct} (not shown). The amount of digested bonds is very subject to the random initialization and the resulting local collagen and crosslinker density. Another factor is partially because a larger k_{ct} leads to a larger density in the center cluster, which then are not influenced by the MMP field. Especially the higher values (above 1) create such big forces that the hoomd model does not have enough time with the used t_{MD} to properly react. Still, it is clear (especially for the lower values of k_{ct}) that the amount of contractile force influences the number of remaining bonds, protected by strain, in the MMP concentration gradient.

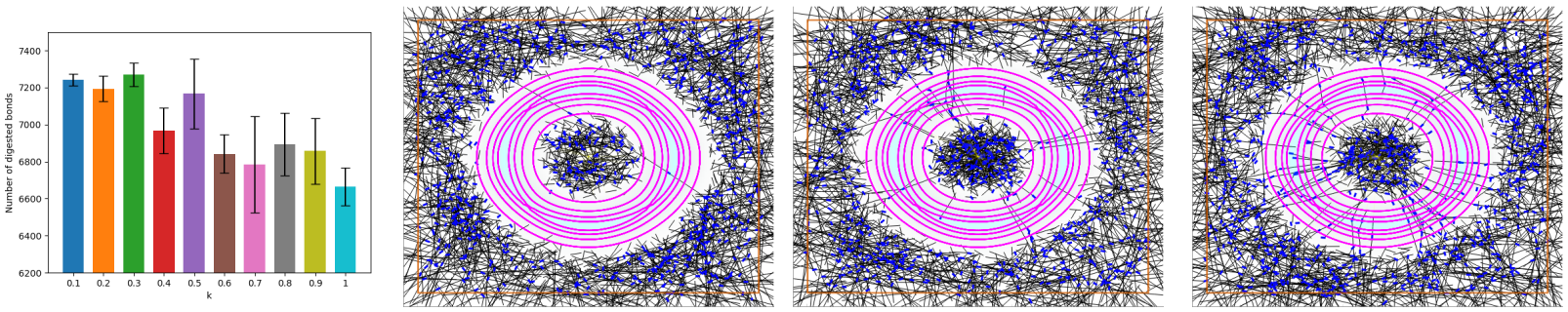

(a) **(b)** **(c)** **(d)**

Figure 19: Simulations with 100 focal adhesions, varying the spring constant k_{ct} of the contractile bonds. 19a shows bar plots with standard deviations of the mean number (3x repeated) of digested bonds at t=260 for a range of k_{ct} between 0.1 and 1.0. Figures 19b to 19d show snapshot examples of three simulations with $k_{ct} =$ 0.1, 0.5, 1.0 at t=260. They show a clear difference in the amount of protected bonds remaining when k_{ct} increases.

4 Discussion

4.1 Results

We studied the dynamics between fibrous collagen ECM and its degradation by collagenases. This was done by extending an existing model for ECM-cell interactions with MMP functionality. This thesis used the key idea that the pathogenic circumstance of inflammation as a part of psoriasis is associated with local changes in ECM structure as a starting point. The dynamics were investigated of how cells restructure and remodel their surrounding ECM through both the production of collagen as well as secretion of collagenases, the compounds responsible for collagen degradation. The property of strain protecting collagen from collagenases is an important factor in this process. In the literature a generalization of this strain-degradation rate relationship was found and selected for use in the thesis [66]. Computational modeling was used as a tool for investigating the local remodeling of the ECM, since it allows for control over various parameters and experimental setup as well as the possibility to combine various parts of earlier research in a way that would not be feasible *in vitro*. An existing model with a discrete PDE layer for and a continuous molecular dynamics layer was used as a basis for an extension, which implements collagen degradation based on the concentration a collagen bond experiences at a given timestep. The model runs consecutively the PDE layer for collagenase secretion, diffusion and degradation, then the molecular dynamics for updating the position of the collagen and finally the degradation of the collagen as a single timestep.
In Section 3.1 the model has been shown to properly integrate the model layers by way of a small scale toy simulation, which shows that a concentration gradient of MMP from a single secretion point correctly degrades the local ECM collagen fibrils.
Sections 3.2 to 3.4 show how an artificially strained network reacts to local degradation of stress bearing collagen fibrils and crosslinkers with a simple concentration threshold based exclusion function. It was first shown that the topology drastically changes due to the recoil of the network after a sudden removal of stress on one side. Afterwards it was investigated how the local density of the network influences this change in topology. While the difference is not very large, low density ECM divides the strain less than

high density ECM, meaning that the recoil effect is amplified.
In Section 3.5 the generalized strain-degradation law 1 is implemented to see how this strain protection law influences collagen degradation. After exposure to an instantaneous uniform concentration of MMP, unstrained bonds are degraded faster than strained bonds. After prolonged exposure, only a strained subnetwork of stress bearing fibrils and crosslinkers remains. Section 3.6 demonstrates how, similarly to the paper the laws are sourced from, there is barely a difference between using degradation law 1 and degradation law 2. The degradation laws are subject to parameters however, so in Section 3.7 the Ξ_{min} parameter is increased. The value of Ξ_{min} correlates with the number of digested bonds after prolonged exposure, but above some point the difference in this number of digested bonds is less noticeable between values of Ξ_{min}. Aside from strain influencing the degradation of collagen, the literature also informs us that the concentration of collagenase influences the degradation rate in a Michaelis-Menten kinetics fashion. The model takes this into account and scales the degradation rate accordingly, shown in Section 3.8 to create a gradient of mean lifetime caused by a gradient of MMP concentration over the simulation space.
After a thorough examination of the models functioning and how changing certain parameters affects its functioning, a shift was made to a scenario which might take place with cells in the ECM of the skin in Section 3.9. To mimic a cell creating local strain through application of contractile force while simultaneously secreting collagenases, contractile forces were applied to collagen at the edge of the "cell" while secreting MMP in this same ring. Using the degradation law to slow down the degradation rate of strained fibrils as well as scaling by the concentration of the MMP field, an area around the cell is transformed from a disorganized ECM to a highly structured ECM. In psoriasis the key observation was the strikingly different collagen structures. The model shows that the implementation of just two cellular processes (straining through contractile force and MMP secretion) causes dynamics that can change the collagen structures significantly. A further investigation on the effect of the amount of contractile force was done to see what balance between the cell and the elasticity of the ECM yields protection of the strained fibrils in Section 3.10. Here a comparison is made between earlier work investigating the effect of the stiffness of the ECM, where a similar balance was explored by perturbing ECM properties. Similar results in the ratio between cell force and ECM force further validate the model.
The thesis incorporates data about collagen degradation from earlier *in vitro* research for *in silico* simulations using the extended model with a scenario which we might expect *in vivo*. These simulations show that a cell can remodel their local ECM effectively using straining forces and secretion of collagenases. Along the way various aspects of the model were investigated, showing a robustness and flexibility which can be harnessed in any future work.

4.2 Limitations

Something important about the extension of the existing computational model is that the models functioning was trusted and not investigated for flaws. Outside of the changed parameters shown in Parameter Table 1, no further examination was done on the other parameters and they were taken as is. Any issues, assumptions or inaccuracies that the original model contained are thus inherited for the extension.
When incorporating the experimental information about the properties of collagen degradation by collagenases, there is an assumption made about how this translates to a situation such as in psoriasis patients. First, the *in vitro* experiments from which the data was sourced were mainly performed using

single or a small number of fibrils, so there is some inference from these experiments to a *in silico* simulation in which this data is used on a way larger scale, with a few thousand fibrils subject to collagenases in a bulk simulation. The second aspect that might not align perfectly is that the *in vitro* experiments were performed with different types of collagenases and collagen. To illustrate this, Table 2 shows different studies on the effect of collagenase on collagen. The table shows that there is barely any consensus in which collagenases and collagen types have been studied which leads to the problem where no quantitative data can be directly compared between the studies due to the variability of circumstances. While these papers report different values with different types of collagenase and collagen, most show similar trends so the assumption is made that an astraction can be used in the form of the Loerakker degradation laws [66] as is.

Author	Collagenase	Collagen type
Adhikari *et al.* [50, 51]	MMP-1	single recombinant modified human collagen I (rHCol1) trimers
Bhole *et al.* [47]	Bacterial collagenase (Clostridium histolyticum)	Bovine type I atelo-collagen
Camp *et al.* [80]	Clostridium histolyticum	rHCol1
Chung *et al.* [49]	Recombinant MMP from an E. coli vector	Guinea pig skin type I collagen
Flynn *et al.* [48]	Recombinant human MMP-8	Bovine type I collagen
Harris and Farrell [81]	"Bacterial or synovial collagenase"	Guinea pig skin collagen
Huang and Yannas [40]	Purified bacterial collagenase (CLSPA)	Bovine tendon reconstituted collagen
Nabeshiba *et al.* [82]	Unspecified bacterial collagenase	Collagen from rabbit patella, patellar tendon and tibia tissues
Ruberti and Hallab [46]	Clostridium histolyticum	Collagen sourced from bovine corneas
Wyatt *et al.* [53]	Unspecified bacterial collagenase	Collagen I from rat tail tendons

Table 2: Table with different publications about the effect of collagenase on collagen under various circumstances. The table highlights the variety of collagen types and collagenases used in these studies, leading to difficulty sourcing reliable quantitative data.

In order to see if the experimental data about collagenase degradation alone is enough to get a local restructuring of the ECM, other factors that might influence this process were consciously left out. These include interactions with proteoglyca in the collagenous fibrous ECM, the activation process between MMP and TIMPs where instead all MMPs that are secreted are always activate and because the experimental data does not inform us about any negative strain, where the fibril is compressed, negative strain is ignored entirely.
It should be taken into account that the concept of strain has a multitude of definitions, so strain is measured differently in different contexts. For the results presented here a simplified linear elastic fibre strain was used as defined in Equation 15. This strain calculation works out fine for the model, but the exact values might not align when comparing results with different papers.
A metric used to quantify the simulation results in a few sections is the order parameter. The order parameter informs us about the alignment of bonds in the network. It should be noted that the order parameter does not seem sensitive to the experiments and should be taken with a grain of salt. The model contains a set of bonds that not all form one network; Sometimes strands simply float around on their own or multiple smaller networks are present. When inspecting the simulations, our brain filters these out to the background as nothing really happens to them, but the order parameter calculation takes them into account and they influence the output. With the current setup of the program, it is not possible to automatically ignore these bonds, since there is nothing inherently different about the floating strands. Some algorithm performing exploration of the network after initialization to see which

bonds are indirectly connected to which bonds and through this identifying strands which do not connect to any others to filter them out could be implemented. This would involve creation of a new module for just this and was determined to be out of scope for this thesis. This means that the global order parameter in Sections 3.2 and 3.3 is rather low compared to the visible change in alignment. The same goes for the local heatmaps from Section 3.4, where the high order parameter values only occur for bins where there are very little bonds. Only when these "background" bonds are eliminated, such as in the contractile force experiments in Sections 3.9 and 3.10 in which the aligned bonds are isolated, we see high order parameter values for high alignments. Moving clusters also influence the order parameter heavily. Because of the local bond density based distribution of crosslinkers in the network, the random networks often contain tangles, which move as a cluster at once. The clusters have bonds sticking out in all directions, so while the tangle might be a part of a structured local ECM, the order parameter reports a very low value for this part of the ECM. A different method of distributing crosslinkers might yield less of these clusters and thus lead the order parameter to more closely match the qualitative results.
For the simulations that approximate the cell contracting, the described method (see Section 2.3.1 relies on an assumption that the cell is perfectly circular at the start. The balance between the contractile force and the ECM is biologically relevant and has been shown to be dependent on cell shape and the distance from the center of the cell [83]. Importantly, the described experimental setup as used in Sections 3.9 and 3.10 does not factor in the biological context of the way cells adhere to the ECM through focal adhesions. In fact, the original model that has been extended was used in a paper investigating just this; how cell contraction and ECM properties interact through focal adhesions [63]. In a sense, this simplified method is an abstracted course graining of their experimental setup.

4.3 Future work

A general interest of what happens in the dermis ECM of psoriasis patients has led to the creation of a general purpose collagen remodeling computational model. With many of the above limitations (Section 4.2) in mind, there are a number of ways future work with this model could be directed, because the model offers itself to many applications and further extensions. This model might help with studying how collagenases affect collagen networks in psoriasis patients, but it is not there yet.
First and most relevant for the psoriasis context is that psoriasis usually occurs at locations which endure repetitive strain (elbows, knees, scalp, etc.). The simulations performed for this thesis only considered a single straining phase, after which or during which secretion and digestion was applied to the network. An experiment setup with repetitive strain might look very different to the general experiment setup used in this thesis and would probably need very different parameter values for for instance the digestion process.
Part of the research was implementation of the Loerakker collagen degradation laws [66] to see how they could influence the model behaviour, but Loerakker's paper also proposed collagen production laws. An important part of ECM restructuring involves not only the (selective) degradation of collagen, but also production of collagen. Production of collagen and also creation/breakage of crosslinkers was out of scope for this thesis, but with some work the model could definitely also include these processes for more extensive investigation into local ECM remodeling.
A limitation noted previously in Section 4.2 is the case of bond compression, which is completely ignored currently. Since collagen behaves springlike, one might think how springs react to compression, which

is usually some shortening followed by bending. This behaviour would be more difficult to recreate in the specific computational model used in this thesis, but would more accurately model collagen under compression instead of only under tension.
The final two results sections (Sections 3.9 and 3.10) attempted to model the effect of a cell on the surrounding ECM, without explicitly modeling the cell itself. While the contractile force properly shrinks the ECM as the "cell" contracts, secretion is done in a stationary ring. Of course, as the cell physically contracts while creating the contractile force, the frontier of where the secretion takes place also shrinks towards the cell center together with the edge of the cell. This dynamic updating of the secretion location is considered out of scope for this thesis, since it would involve some significant changes in how the model communicates information between the different layers. Adding to this, some unpublished work has been done on the model during the thesis process which might replace the functionality through integration of the CPM layer of the model so double work would have been done. Due to the modular nature of the model extension (as desired by the research group), these new developments could be combined with the implementations from this thesis for further research.
In the latter of these sections (Section 3.10), the effect of different contractile force levels was investigated with a limited number of focal adhesions which would endure the force. These simulations were to mirror work done in Tsingos *et al.* [63], but looking at the force balance from the point of view of the cell instead of the ECM. Importantly, the paper investigated the balance for a range of focal adhesion counts. For simplicity, this was not done in this thesis but could yield some more interesting insights. This subject of force harmonics and balances in the ECM is an entire field of research on its own (e.g. [83]) and the point of the section and experiments was simply to see how the cell could affect collagen protection by modulating the exerted force. The model could be used to take this much further, but this would be reserved for future work.
The last option for future work might be including dynamics between multiple cells which all apply forces to the ECM which could lead to some very interesting dynamics, for instance: How much less force would multiple cells individually need to apply to reach a similar level of ECM protection as a single cell does? Does the influence of multiple cells lead to different protected collagen structures than we have seen in this thesis? One might want to extend the model further first or simply go into the multi-cell scenario with the current implementation, the options are endless.

5 Conclusion

In this thesis, the effect of MMPs on stressed ECM is modeled using a computational model. The context of the disease psoriasis with its dyregulated ECM in the dermis is taken as a starting point. The dysregulation entails some local change of the fibrous ECM scaffold into a more organized pattern associated with changed cell motility and tissue invasion. Local ECM remodeling occurs partially through collagen digestion by MMPs, a process which is subject to a number of factors. This collagen digestion process is scrutinized in this thesis.
An existing computational model with a molecular dynamics layer modeling collagen as well as a PDE layer modeling compound concentrations is extended. The extension includes ways to induce artificial strain and a module for collagen digestion based on the MMP concentration that incorporates experimental data about collagen-strain protection.
Using this model, a number of experiments were carried out to see how this extension influences the

model behaviour, showing how collagen can correctly be degraded by MMP and how this process has effects on topology by removal of stresses. These effects cascade through the rest of the network, based on stress levels and collagen density. Afterwards experiments on the influence of strain and concentration gradients were done, showing that the model can use experimentally derived degradation laws and concentration levels to influence collagenase degradation rates. Finally a set of experiments were done to actually simulate a situation one might encounter in psoriasis patients, where cells apply forces to the ECM to strain it while simultaneously secreting MMPs to digest and remove unstrained collagen.
In this thesis it is shown how known experimental data about the effects of MMP on collagen together with an approximation on how cells apply forces to the ECM can effectively locally remodel the ECM around the cell. To get to this point, a number of aspects about the model are explored to see how the model reacts to perturbations and if it still holds and follows expectations. Through this, a few avenues of future work are available using the model as a basis. The thesis started as a general insight in psoriasis ECM dysregulation by MMPs, continued as an exploration about the effects of MMP during the remodeling process and the resulting model might be used for many more contexts involving ECM remodeling.

References

[1] N. Weigle and S. McBane, "Psoriasis," *American Family Physician*, vol. 87, pp. 626–633, May 2013.

[2] L. Burfield and A. Burden, "Psoriasis," *Journal of the Royal College of Physicians of Edinburgh*, vol. 43, no. 4, pp. 334–339, 2013.

[3] T. McCormick, N. Ayala-Fontanez, and D. Soler, "Current knowledge on psoriasis and autoimmune diseases," *Psoriasis: Targets and Therapy*, p. 7, Feb. 2016.

[4] C. E. M. Griffiths, "Psoriasis 1 Pathogenesis and clinical features of psoriasis," *The Lancet*, vol. 370, 2007.

[5] Subcommittee on Immunotoxicology, Committee on Biologic Markers, Board on Environmental Studies and Toxicology, National Research Council, *Biologic Markers in Immunotoxicology*. 1 ed., 1992.

[6] Ş. B. Tönük and Z. R. Yorgancıoğlu, "Biomechanical Factors in Psoriatic Disease: Defective Repair Exertion as a Potential Cause. Hypothesis Presentation and Literature Review," *ACR Open Rheumatology*, vol. 1, pp. 452–461, Sept. 2019.

[7] J. Moll and V. Wright, "Psoriatic arthritis," *Seminars in Arthritis and Rheumatism*, vol. 3, pp. 55–78, Jan. 1973.

[8] K. Pfisterer, L. E. Shaw, D. Symmank, and W. Weninger, "The Extracellular Matrix in Skin Inflammation and Infection," *Frontiers in Cell and Developmental Biology*, vol. 9, p. 682414, July 2021.

[9] A. D. Theocharis, S. S. Skandalis, C. Gialeli, and N. K. Karamanos, "Extracellular matrix structure," *Advanced Drug Delivery Reviews*, vol. 97, pp. 4–27, Feb. 2016.

[10] C. Frantz, K. M. Stewart, and V. M. Weaver, "The extracellular matrix at a glance," *Journal of Cell Science*, vol. 123, pp. 4195–4200, Dec. 2010.

[11] M. D. Shoulders and R. T. Raines, "Collagen Structure and Stability," *Annual Review of Biochemistry*, vol. 78, pp. 929–958, June 2009.

[12] P. Yadav, "Biomedical Biopolymers, their Origin and Evolution in Biomedical Sciences: A Systematic Review," *Journal of Clinical and Diagnostic Research*, 2015.

[13] S. Ricard-Blum, "The Collagen Family," *Cold Spring Harbor Perspectives in Biology*, vol. 3, pp. a004978–a004978, Jan. 2011.

[14] B. Yue, "Biology of the Extracellular Matrix: An Overview," *Journal of Glaucoma*, vol. 23, pp. S20–S23, 2014.

[15] M. Wu, K. Cronin, and J. S. Crane, "Biochemistry, Collagen Synthesis," *StatPearls*, 2022.

[16] P. Bruckner, "Suprastructures of extracellular matrices: paradigms of functions controlled by aggregates rather than molecules," *Cell and Tissue Research*, vol. 339, pp. 7–18, Jan. 2010.

[17] K. E. Kadler, Hojima, Y, and Prockop, D J, "Assembly of collagen fibrils de novo by cleavage of the type I pC-collagen with procollagen C-proteinase. Assay of critical concentration demonstrates that collagen self-assembly is a classical example of an entropy-driven process.," *The Journal of Biological Chemistry*, vol. 260, pp. 15696–15701, May 1987.

[18] D. F. Holmes, Y. Lu, T. Starborg, and K. E. Kadler, "Collagen Fibril Assembly and Function," in *Current Topics in Developmental Biology*, vol. 130, pp. 107–142, Elsevier, 2018.

[19] T. Wess, "Collagen Fibril Form and Function," in *Advances in Protein Chemistry*, vol. 70, pp. 341–374, Elsevier, 2005.

[20] J. P. R. O. Orgel, T. C. Irving, A. Miller, and T. J. Wess, "Microfibrillar structure of type I collagen in situ," *Proceedings of the National Academy of Sciences*, vol. 103, pp. 9001–9005, June 2006.

[21] J. S. Bell, S. Hayes, C. Whitford, J. Sanchez-Weatherby, O. Shebanova, N. J. Terrill, T. L. M. Sørensen, A. Elsheikh, and K. M. Meek, "Tropocollagen springs allow collagen fibrils to stretch elastically," *Acta Biomaterialia*, 2022.

[22] S. Motte and L. J. Kaufman, "Strain stiffening in collagen I networks," *Biopolymers*, vol. 99, pp. 35–46, Jan. 2013.

[23] K. A. Jansen, A. J. Licup, A. Sharma, R. Rens, F. C. MacKintosh, and G. H. Koenderink, "The Role of Network Architecture in Collagen Mechanics," *Biophysical Journal*, vol. 114, pp. 2665–2678, June 2018.

[24] N. A. S. Manssor, Z. Radzi, N. A. Yahya, L. Mohamad Yusof, F. Hariri, N. H. Khairuddin, N. H. Abu Kasim, and J. T. Czernuszka, "Characteristics and Young's Modulus of Collagen Fibrils from Expanded Skin Using Anisotropic Controlled Rate Self-Inflating Tissue Expander," *Skin Pharmacology and Physiology*, vol. 29, no. 2, pp. 55–62, 2016.

[25] K. K. Dwivedi, P. Lakhani, S. Kumar, and N. Kumar, "Effect of collagen fibre orientation on the Poisson's ratio and stress relaxation of skin: an ex vivo and in vivo study," *Royal Society Open Science*, vol. 9, 2022.

[26] M. P. Wenger, L. Bozec, M. A. Horton, and P. Mesquida, "Mechanical Properties of Collagen Fibrils," *Biophysical Journal*, vol. 93, pp. 1255–1263, Aug. 2007.

[27] V. W. Tang, "Collagen, stiffness, and adhesion: the evolutionary basis of vertebrate mechanobiology," *Molecular Biology of the Cell*, vol. 31, pp. 1823–1834, Aug. 2020.

[28] M. L. Gardel, I. C. Schneider, Y. Aratyn-Schaus, and C. M. Waterman, "Mechanical Integration of Actin and Adhesion Dynamics in Cell Migration," *Annual Review of Cell and Developmental Biology*, vol. 26, pp. 315–333, Nov. 2010.

[29] W. Li, J. Fan, M. Chen, and D. T. Woodley, "Mechanisms of human skin cell motility," *Histology and Histopathology*, vol. 19, pp. 1311–1324, 2004.

[30] A. E. Miller, P. Hu, and T. H. Barker, "Feeling things out: bidirectional signaling of the cell–ECM interface, implications in the mechanobiology of cell spreading, migration, proliferation, and differentiation," *Advanced healthcare materials*, vol. 9, no. 8, p. 1901445, 2020. Publisher: Wiley Online Library.

[31] J. Gross and C. M. Lapiere, "Collagenolytic Activity in Amphibian Tissues: A Tissue Culture Assay," *Proceedings of the National Academy of Sciences*, vol. 48, pp. 1014–1022, June 1962.

[32] H. Nagase and J. F. Woessner, "Matrix Metalloproteinases," *Journal of Biological Chemistry*, vol. 274, pp. 21491–21494, July 1999.

[33] R. Visse and H. Nagase, "Matrix Metalloproteinases and Tissue Inhibitors of Metalloproteinases: Structure, Function, and Biochemistry," *Circulation Research*, vol. 92, pp. 827–839, May 2003.

[34] H. Nagase, R. Visse, and G. Murphy, "Structure and function of matrix metalloproteinases and TIMPs," *Cardiovascular Research*, vol. 69, pp. 562–573, Feb. 2006.

[35] H. E. Van Wart and H. Birkedal-Hansen, "The cysteine switch: a principle of regulation of metalloproteinase activity with potential applicability to the entire matrix metalloproteinase gene family.," *Proceedings of the National Academy of Sciences*, vol. 87, pp. 5578–5582, July 1990.

[36] K. Brew, D. Dinakarpandian, and H. Nagase, "Tissue inhibitors of metalloproteinases: evolution, structure and function," *Biochimica et Biophysica Acta (BBA) - Protein Structure and Molecular Enzymology*, vol. 1477, pp. 267–283, Mar. 2000.

[37] K. Kessenbrock, V. Plaks, and Z. Werb, "Matrix Metalloproteinases: Regulators of the Tumor Microenvironment," *Cell*, vol. 141, pp. 52–67, Apr. 2010.

[38] P. Lu, K. Takai, V. M. Weaver, and Z. Werb, "Extracellular Matrix Degradation and Remodeling in Development and Disease," *Cold Spring Harbor Perspectives in Biology*, vol. 3, pp. a005058–a005058, Dec. 2011.

[39] M. Gisslow and B. McBride, "A rapid sensitive collagenase assay," *Analytical Biochemistry*, vol. 68, pp. 70–78, Sept. 1975.

[40] C. Huang and I. V. Yannas, "Mechanochemical studies of enzymatic degradation of insoluble collagen fibers," *Journal of Biomedical Materials Research*, vol. 11, no. 1, pp. 137–154, 1977. _eprint: https://onlinelibrary.wiley.com/doi/pdf/10.1002/jbm.820110113.

[41] T. Hayashi, T. Nakamura, H. Horj, and Y. Nagai, "The Degradation Rates of Type I, n , and III Collagens by Tadpole Collagenase," *The Journal of Biochemistry*, vol. 87, no. 3, pp. 809–815, 1980.

[42] B. Johnson-Wint, "A quantitative collagen film collagenase assay for large numbers of samples," *Analytical Biochemistry*, vol. 104, pp. 175–181, May 1980.

[43] G. Fields, H. Van Wart, and H. Birkedal-Hansen, "Sequence specificity of human skin fibroblast collagenase. Evidence for the role of collagen structure in determining the collagenase cleavage site.," *Journal of Biological Chemistry*, vol. 262, pp. 6221–6226, May 1987.

[44] K. Hasty, J. Jeffrey, M. Hibbs, and H. Welgus, "The collagen substrate specificity of human neutrophil collagenase.," *Journal of Biological Chemistry*, vol. 262, pp. 10048–10052, July 1987.

[45] S.-W. Chang and M. J. Buehler, "Molecular biomechanics of collagen molecules," *Materials Today*, vol. 17, pp. 70–76, Mar. 2014.

[46] J. W. Ruberti and N. J. Hallab, "Strain-controlled enzymatic cleavage of collagen in loaded matrix," *Biochemical and Biophysical Research Communications*, vol. 336, pp. 483–489, Oct. 2005.

[47] A. P. Bhole, B. P. Flynn, M. Liles, N. Saeidi, C. A. Dimarzio, and J. W. Ruberti, "Mechanical strain enhances survivability of collagen micronetworks in the presence of collagenase: implications for load-bearing matrix growth and stability," *Philosophical Transactions of the Royal Society A: Mathematical, Physical and Engineering Sciences*, vol. 367, pp. 3339–3362, Sept. 2009.

[48] B. P. Flynn, A. P. Bhole, N. Saeidi, M. Liles, C. A. DiMarzio, and J. W. Ruberti, "Mechanical Strain Stabilizes Reconstituted Collagen Fibrils against Enzymatic Degradation by Mammalian Collagenase Matrix Metalloproteinase 8 (MMP-8)," *PLoS ONE*, vol. 5, p. e12337, Aug. 2010.

[49] L. Chung, D. Dinakarpandian, N. Yoshida, J. L. Lauer-Fields, G. B. Fields, R. Visse, and H. Nagase, "Collagenase unwinds triple-helical collagen prior to peptide bond hydrolysis," *The EMBO Journal*, vol. 23, pp. 3020–3030, Aug. 2004.

[50] A. S. Adhikari, J. Chai, and A. R. Dunn, "Mechanical Load Induces a 100-Fold Increase in the Rate of Collagen Proteolysis by MMP-1," *Journal of the American Chemical Society*, vol. 133, pp. 1686–1689, Feb. 2011.

[51] A. S. Adhikari, E. Glassey, and A. R. Dunn, "Conformational Dynamics Accompanying the Proteolytic Degradation of Trimeric Collagen I by Collagenases," *Journal of the American Chemical Society*, vol. 134, pp. 13259–13265, Aug. 2012.

[52] P. S. Nerenberg, R. Salsas-Escat, and C. M. Stultz, "Do collagenases unwind triple-helical collagen before peptide bond hydrolysis? Reinterpreting experimental observations with mathematical models," *Proteins: Structure, Function, and Bioinformatics*, vol. 70, pp. 1154–1161, Mar. 2008.

[53] K. E.-K. Wyatt, J. W. Bourne, and P. A. Torzilli, "Deformation-dependent enzyme mechanokinetic cleavage of type I collagen," *Journal of biomechanical engineering*, vol. 131, p. 051004, May 2009.

[54] C. C. van Donkelaar, T. a. M. Heck, W. Wilson, J. Foolen, and K. Ito, "Versatility of a Collagen Adaptation Model That Includes Strain-Dependent Degeneration and Cell Traction," American Society of Mechanical Engineers Digital Collection, Jan. 2014.

[55] R. M. H. Merks, S. A. Newman, and J. A. Glazier, "Cell-Oriented Modeling of In Vitro Capillary Development," in *Cellular Automata*, vol. 3305, pp. 425–434, Berlin, Heidelberg: Springer Berlin Heidelberg, 2004. Series Title: Lecture Notes in Computer Science.

[56] J. A. Glazier and F. Graner, "Simulation of the differential adhesion driven rearrangement of biological cells," *Physical Review E*, vol. 47, pp. 2128–2154, Mar. 1993.

[57] A. Gamba, D. Ambrosi, A. Coniglio, A. De Candia, S. Di Talia, E. Giraudo, G. Serini, L. Preziosi, and F. Bussolino, "Percolation, Morphogenesis, and Burgers Dynamics in Blood Vessels Formation," *Physical Review Letters*, vol. 90, p. 118101, Mar. 2003.

[58] G. Serini, D. Ambrosi, E. Giraudo, A. Gamba, L. Preziosi, and F. Bussolino, "Modeling the early stages of vascular network assembly," *The EMBO Journal*, vol. 22, pp. 1771–1779, Apr. 2003.

[59] R. M. Merks and J. A. Glazier, "A cell-centered approach to developmental biology," *Physica A: Statistical Mechanics and its Applications*, vol. 352, pp. 113–130, July 2005.

[60] J. T. Daub and R. M. H. Merks, "A Cell-Based Model of Extracellular-Matrix-Guided Endothelial Cell Migration During Angiogenesis," *Bulletin of Mathematical Biology*, vol. 75, pp. 1377–1399, Aug. 2013.

[61] I. Niculescu, J. Textor, and R. J. De Boer, "Crawling and Gliding: A Computational Model for Shape-Driven Cell Migration," *PLOS Computational Biology*, vol. 11, p. e1004280, Oct. 2015.

[62] S. de Bruin, "Modelling the influence of extracellular polymeric substances in aerobic granule morphology," 2018.

[63] E. Tsingos, B. H. Bakker, K. A. Keijzer, H. J. Hupkes, and R. M. Merks, "Hybrid cellular Potts and bead-spring modeling of cells in fibrous extracellular matrix," *Biophysical Journal*, vol. 122, pp. 2609–2622, July 2023.

[64] T. Ristori, A. Vigliotti, F. P. Baaijens, S. Loerakker, and V. S. Deshpande, "Prediction of cell alignment on cyclically strained grooved substrates," *Biophysical journal*, vol. 111, no. 10, pp. 2274–2285, 2016. Publisher: Elsevier.

[65] R. F. M. Van Oers, E. G. Rens, D. J. LaValley, C. A. Reinhart-King, and R. M. H. Merks, "Mechanical Cell-Matrix Feedback Explains Pairwise and Collective Endothelial Cell Behavior In Vitro," *PLoS Computational Biology*, vol. 10, p. e1003774, Aug. 2014.

[66] S. Loerakker, C. Obbink-Huizer, and F. P. Baaijens, "A physically motivated constitutive model for cell-mediated compaction and collagen remodeling in soft tissues," *Biomechanics and modeling in mechanobiology*, vol. 13, pp. 985–1001, 2014. Publisher: Springer.

[67] S. Loerakker, T. Ristori, and F. P. Baaijens, "A computational analysis of cell-mediated compaction and collagen remodeling in tissue-engineered heart valves," *Journal of the Mechanical Behavior of Biomedical Materials*, vol. 58, pp. 173–187, May 2016.

[68] A. G. Hoekstra, B. Chopard, D. Coster, S. Portegies Zwart, and P. V. Coveney, "Multiscale computing for science and engineering in the era of exascale performance," *Philosophical Transactions of the Royal Society A: Mathematical, Physical and Engineering Sciences*, vol. 377, p. 20180144, Apr. 2019.

[69] J. A. Anderson, J. Glaser, and S. C. Glotzer, "HOOMD-blue: A Python package for high-performance molecular dynamics and hard particle Monte Carlo simulations," *Computational Materials Science*, vol. 173, p. 109363, Feb. 2020.

[70] J. W. Reinhardt and K. J. Gooch, "Agent-Based Modeling Traction Force Mediated Compaction of Cell-Populated Collagen Gels Using Physically Realistic Fibril Mechanics," *Journal of Biomechanical Engineering*, vol. 136, pp. 021–024, Feb. 2014.

[71] J. W. Reinhardt and K. J. Gooch, "An Agent-Based Discrete Collagen Fiber Network Model of Dynamic Traction Force-Induced Remodeling," *Journal of Biomechanical Engineering*, vol. 140, p. 051003, May 2018.

[72] M. L. V. Pitteway, "Algorithm for drawing ellipses or hyperbolae with a digital plotter," *The Computer Journal*, vol. 10, pp. 282–289, Mar. 1967.

[73] J. E. Bresenham, "Algorithm for computer control of a digital plotter," *IBM Systems Journal*, vol. 4, no. 1, pp. 25–30, 1965.

[74] J. C. Craig, "We Must Draw the Line." `https://jccraig.medium.com/we-must-draw-the-line-1820d49d19dd`, Jan. 2022.

[75] I. E. Collier, W. Legant, B. Marmer, O. Lubman, S. Saffarian, T. Wakatsuki, E. Elson, and G. I. Goldberg, "Diffusion of MMPs on the Surface of Collagen Fibrils: The Mobile Cell Surface – Collagen Substratum Interface," *PLoS ONE*, vol. 6, p. e24029, Sept. 2011.

[76] Paul Bourke, "CONREC - A Countouring Subroutine," *Byte*, vol. 12, p. 143, July 1987.

[77] J. P. Borthagaray, R. H. Nochetto, and S. W. Walker, "A structure-preserving FEM for the uniaxially constrained Q-tensor model of nematic liquid crystals," *Numerische Mathematik*, vol. 145, pp. 837–881, Aug. 2020.

[78] S. Marcotti, D. Belo De Freitas, L. D. Troughton, F. N. Kenny, T. J. Shaw, B. M. Stramer, and P. W. Oakes, "A Workflow for Rapid Unbiased Quantification of Fibrillar Feature Alignment in Biological Images," *Frontiers in Computer Science*, vol. 3, p. 745831, Oct. 2021.

[79] S. Li, J.-L. Guan, and S. Chien, "Biochemistry and Biomechanics of Cell Motility," *Annual Review of Biomedical Engineering*, vol. 7, pp. 105–150, Aug. 2005.

[80] R. J. Camp, M. Liles, J. Beale, N. Saeidi, B. P. Flynn, E. Moore, S. K. Murthy, and J. W. Ruberti, "Molecular Mechanochemistry: Low Force Switch Slows Enzymatic Cleavage of Human Type I Collagen Monomer," *Journal of the American Chemical Society*, vol. 133, pp. 4073–4078, Mar. 2011.

[81] E. D. Harris and M. E. Farrell, "Resistance to collagenase: A characteristic of collagen fibrils cross-linked by formaldehyde," *Biochimica et Biophysica Acta (BBA) - Protein Structure*, vol. 278, pp. 133–141, Aug. 1972.

[82] Y. Nabeshima, E. S. Grood, A. Sakurai, and J. H. Herman, "Uniaxial tension inhibits tendon collagen degradation by collagenase *in vitro*," *Journal of Orthopaedic Research*, vol. 14, pp. 123–130, Jan. 1996.

[83] C. A. Lemmon and L. H. Romer, "A Predictive Model of Cell Traction Forces Based on Cell Geometry," *Biophysical Journal*, vol. 99, pp. L78–L80, Nov. 2010.

A Effect of diffusion distance on network

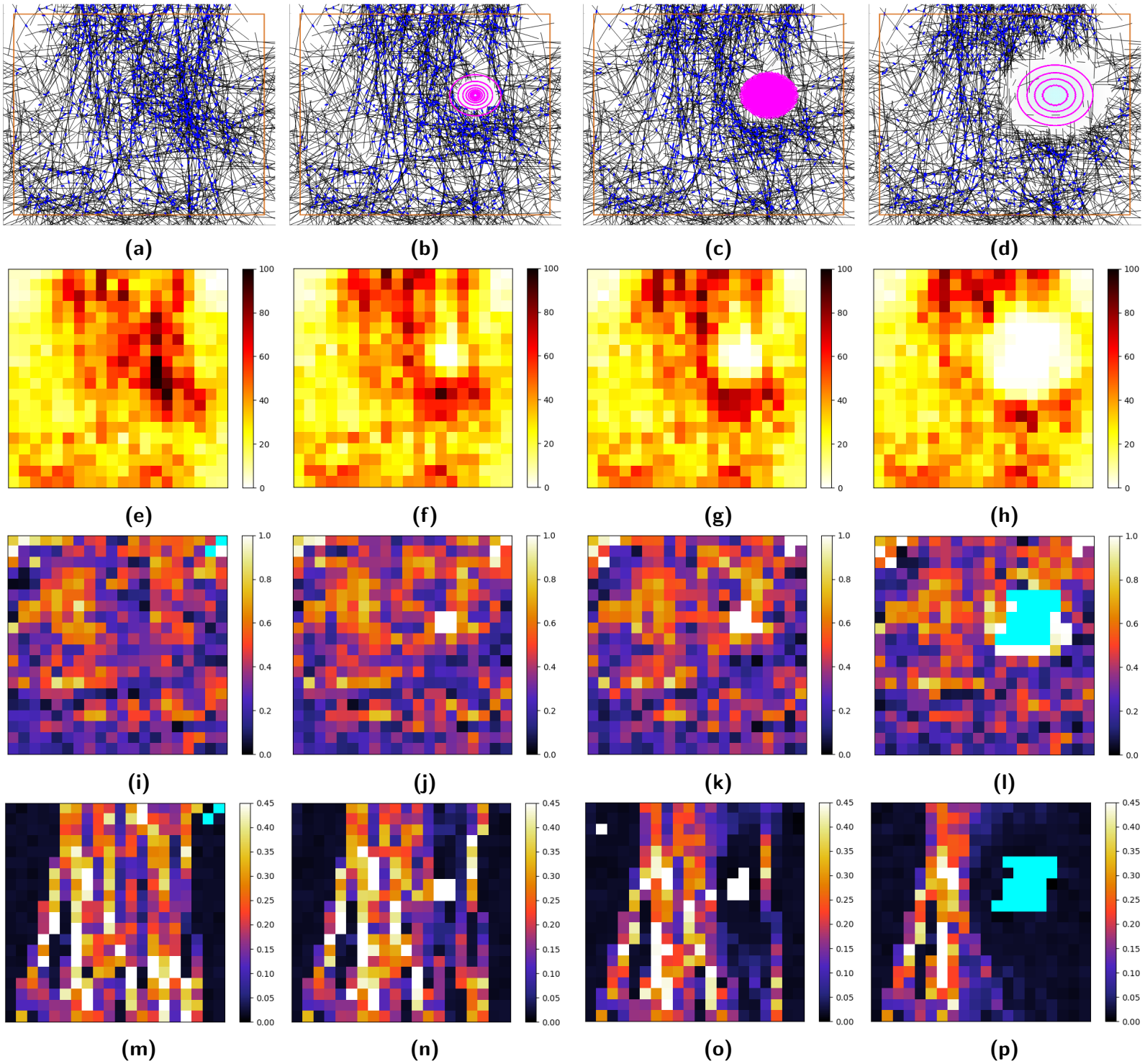

Figure 20: Comparison of the effect of diffusion coefficient D on topology changes in the same network. The rows show the same properties as in figure 11. Each column represents the same timestep. The leftmost column shows the strained network without any MMP added, with the other columns showing secretion in the high density area with TST D=5e-13, D=5.025e-13, D=5.05e-13 from left to right. All columns are from t=319, except the rightmost column which has t=271 (and is identical to the rightmost column from Figure 11). Heatmap bins without any bonds are coloured cyan. This comparison shows why a larger D was chosen to show the effects of collagen density on the impact MMP has on the topology of the network. The simulations where D is smaller, it causes the area of effect for the digestion of collagen to be smaller. Because of the lower amount of stresses being removed the network topology changes less.

B Contractile force secretion radius

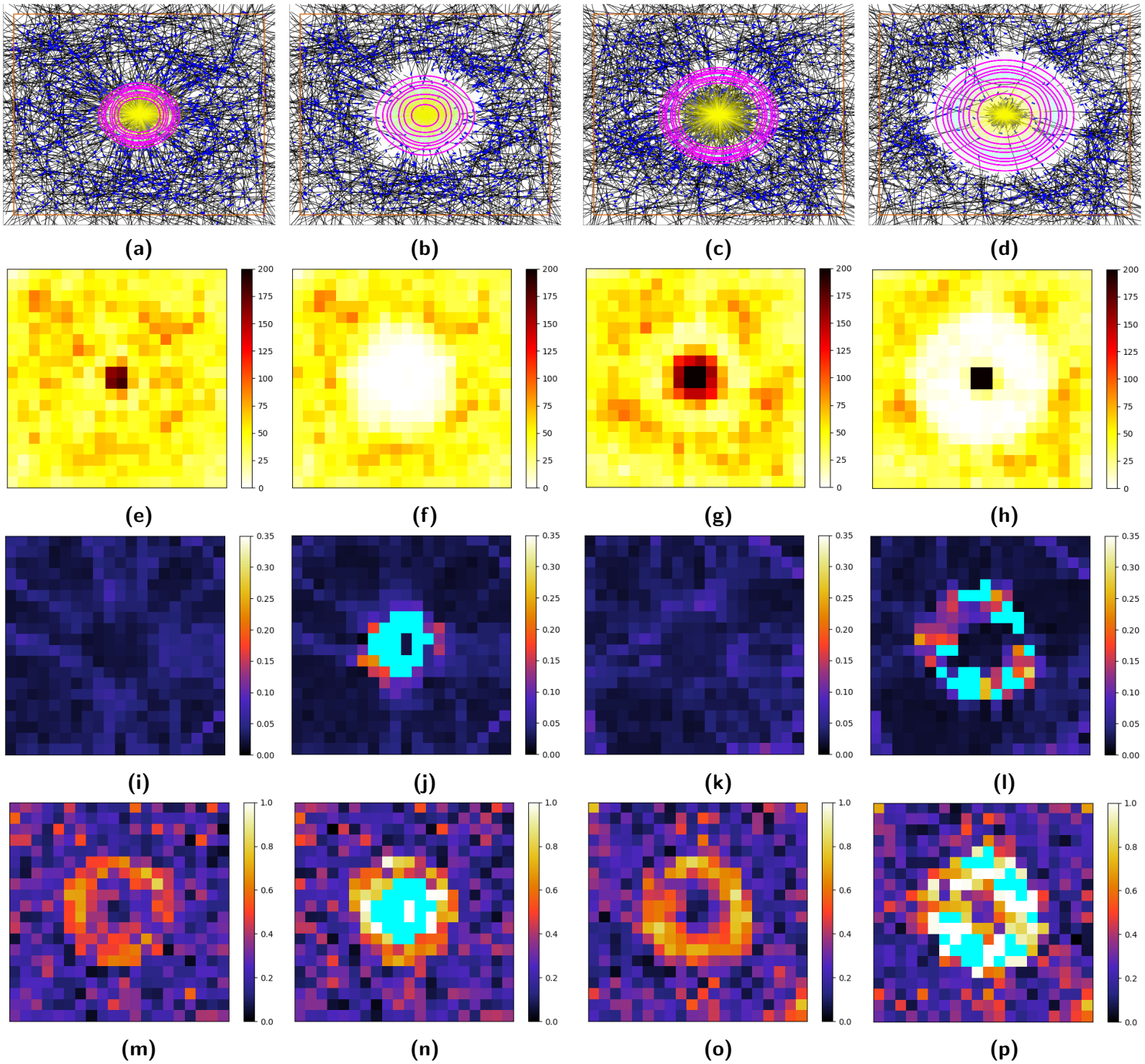

Figure 21: Snapshots of two simulations from experiments on finding a reasonable secretion radius. The rows show the same properties as in Figure 18. The left two columns show snapshots of a simulation with radius 25, the right two columns show snapshots of a simulation with radius 40. The snapshots are of t=86 and t=260 for both simulations. Heatmap bins without any bonds are coloured cyan. These simulations show that a smaller radius than the value of 50 (which was selected for further experimentation) cause MMPs to encroach on the center cluster before straining can properly protect the bonds. MMPs thus destroy the bonds which would exert stresses on the surrounding network. This destruction is less complete for radius 40 than for radius 25, so the effect of strained bonds remaining is more clear with a larger secretion radius.